



**CHARACTERIZATION OF LASER SPOT WELDS FOR HIGH-SPEED
ELECTRICAL MOTORS**

Lappeenranta–Lahti University of Technology LUT

Master's Programme in Mechanical Engineering, Master's thesis

2025

Meisam Nasr

Examiners: Docent Ilkka Poutiainen

Atharv Agarwal, M.Sc. (Tech.)

ABSTRACT

Lappeenranta–Lahti University of Technology LUT

LUT School of Energy Systems

Mechanical Engineering

Meisam Nasr

Characterization of laser spot welds for high-speed electrical motors

Master's thesis

2025

67 pages, 44 figures, 9 tables and - appendices

Examiners: Docent Ilkka Poutiainen and Atharv Agarwal M.Sc. (Tech.)

Keywords: Laser Spot welding, LSW, Synchronous Reluctance Motors, SynRM, Spot protrusions, Taguchi method

This thesis explores the characteristics of laser spot welded joints in thin-sheet stacks of synchronous reluctance motors (SynRM) rotors. Since electrical motors do not directly rely on fossil fuels, they are considered a major technology for sustainable energy solutions. Synchronous reluctance motors operate without the need for permanent magnet, eliminating their dependency on rare-earth materials. These characteristics enhance their suitability for sustainable approach and further optimization. Laminated structure is typically a standard practice in electrical motor design and construction. This thesis investigated laser spot welding as a novel method of joining dissimilar thin sheet materials, where a stainless steel (316L) supporting layer was sandwiched between two ferromagnetic thin sheets of mild steel (340LA). Laser core power, ring power and interaction time were considered the main parameters of laser welding. The Taguchi method was used for the design of experiments, core power was kept constant, where ring power was changed at four levels and interaction time at two levels. This study evaluated the effects of these parameters on laser spot welds (LSW) protrusion, mechanical strength and failure mode.

All spot protrusion from surface were measured utilizing a laser profilometer. Despite controlled weld parameters, spot protrusion exhibited significant variability with occasional outliers. The tensile-shear test indicated that higher laser power and interaction time led to a significant increase in maximum force and strain values, indicating enhanced mechanical strength of LSWs. The failure mode transitioned from shear at lower laser power to tensile at higher laser power. The cross-section evaluation demonstrated a general upward trend in the average interfacial area between thin sheet layers.

ACKNOWLEDGEMENTS

I would like to express appreciation to my supervisor, Docent Ilkka Poutiainen, the Head of the Laser Laboratory at LUT University, for the opportunity, guidance, technical support, and feedback on this thesis work. I am deeply thankful to my co-supervisor, Atharv Agarwal, M.Sc, junior researcher, for his invaluable feedback, continuous support and practical assistance. I am especially grateful to the REALMachine for supporting this research. I extend my deepest thanks to my beloved wife for her encouragement and support during challenging times. Special and heartfelt thanks to my adorable daughter, whose presence has been my constant inspiration and motivation.

Meisam Nasr

31.03.2025

SYMBOLS AND ABBREVIATIONS

Greek characters

λ	Wavelength	mm
ϕ_c	Core Power Size	μm
ϕ_r	Ring Power Size	μm

Abbreviations

ALA	Axially Laminated Anisotropic
ANOVA	Analysis of Variance
BLR	Bridgeless Rotor
DOE	Design of Experiment
EB	Electron Beam
EV	Electrical Vehicle
HAZ	Heat Affected Zone
ICM	Intermetallic Compound
IM	Induction Motor
LSW	Laser Spot Welding
MS	Mild Steel
PM	Permanent Magnet
SCR	Superimposed Core and Ring-shaped
SS	Stainless Steel
SynRM	Synchronous Reluctance Motor

Table of contents

Abstract

Acknowledgements

Symbols and abbreviations

1	Introduction	7
1.1	Background	7
1.2	Research Question and Methodology	8
1.3	Scope.....	9
2	Literature Review	10
2.1	Synchronous Reluctance Motors?	10
2.1.1	Application of Synchronous Reluctance Motors	11
2.1.2	Construction Methods for Rotors	13
2.2	Laser Welding.....	17
2.2.1	Laser beam shapes	18
2.2.2	Core and Ring-shape Laser welding.....	19
2.2.3	Laser Welding in electrical motors	20
2.2.4	Laser Spot Welding	21
3	Materials and Methods	25
3.1	Materials	25
3.2	Experimental methods	27
3.2.1	Laser System.....	27
3.2.2	Optical Microscope.....	28
3.2.3	Laser Profilometer	29
3.2.4	Tensile Test.....	29
4	Experiments.....	31
4.1	Preliminary Studies.....	31
4.1.1	First run.....	31
4.1.2	Second Run	33
4.1.3	Third Run.....	33

4.1.4	Fourth Run	34
4.1.5	Fifth Run	35
4.2	Tests and Measurements	37
4.2.1	Design of Experiments (DOE).....	37
4.2.2	Test Execution	38
5	Results	41
5.1	Maximum weld protrusion measurement	41
5.2	Tensile-Shear Test	45
5.3	Cross Section of Weld Spots	53
5.4	Statistical Analysis for Taguchi design	58
5.5	Summary.....	61
6	Conclusion.....	63
6.1	Further Research	63
	References.....	65

1 Introduction

The global attitude of engineering industries has evolved to embrace approaches such as sustainability, environmental responsibility, and innovation in manufacturing methods. While humans strive to decrease dependence on fossil fuels, electrical motors play a significant role in this area. Since they do not burn fossil fuel directly, they help to reduce carbon emission and footprint. Synchronous Reluctance Motors (SynRM), among different kinds of motors do not rely on Rare-earth materials, therefore, they are valuable choice for sustainable and environmentally friendly applications. New design and innovative manufacturing methods have enhanced their functionality, performance and efficiency. This thesis focuses on utilizing laser spot welding as a novel method to attach multiple rotor layers for synchronous reluctance motors.

1.1 Background

Although electrical motors are utilized in several industries, as they have wide-scale applications and relatively high efficiency, they still experience some challenges that could affect their operations. Formation of eddy current in the laminated disks of the rotors is one of the major challenges faced when conductive materials within the rotor face fluctuating magnetic fields. The losses and heat generated, especially at high speeds, lead to a reduction in efficiency and demagnetization (Singh, Petrov, Sergeant & Pyrhonen, 2024, p. 1).

Excessive mechanical and thermal loading in high-speed motors can lead to deformation, cracks, or even undesired functional failure. Additionally, vibration and noise are common challenges, caused by cogging torque factors. These vibrations may cause pre-mature wear, reduced performance, and in extreme circumstances also a total failure of motors. Vibrations can also result high operational noise which is not desired in quiet all operation applications such electrical vehicles and household appliances.

Several novel design and manufacturing methods have been utilized to reduce the challenges faced by electrical motors. Keeping in mind the challenges and risks, the selected manufacturing method for the construction of the rotors should be robust and precise.

In this study, laser spot welding is employed and explored as a novel technique to attach rotor sheets, due to precision and the possibility of joining different materials with minimal thermal distortion.

1.2 Research Question and Methodology

The critical role of rotors in Synchronous Reluctance Motors to achieve desired performance increases the importance of its manufacturing and the integrity of its multiple-layers structure as stated. This research aims to investigate how laser spot welding could be utilized to join the thin layers of rotors.

This is a novel method to attach these laminates of SynRMs' rotors, and the question would be whether this technique achieves:

- Required tensile strength with maximum process stability.
- Minimum bead protrusions over the weld face requiring minimum post processing.

The study consists of a thorough literature review, followed by a brief introduction to the materials and methods used in this study, a systematic experimental campaign, and characterization of the welds using scientific methods. Finally, the characterization results are discussed, and future work is suggested. In the literature review, brief aspects about the principle and construction of the SynRM motor are discussed, laser welding in general is investigated, followed by technical aspects of laser spot welding. The experimental section discusses the preliminary studies to obtain a suitable process window and Design of the Experiments (DOE) methodologies used. Finally, these welds are then characterized using tensile testing, laser profiling and weld cross-section evaluation. The research methodology and relations between the steps used in this thesis is demonstrated in Figure 1.

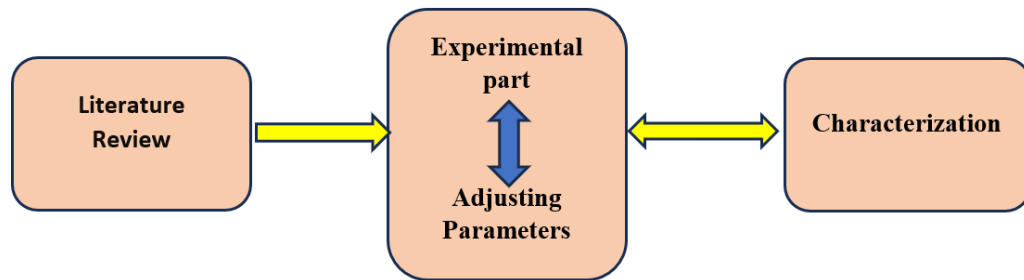


Figure 1. Research Methodology

1.3 Scope

The research is defined to assess the parameters that affect the quality and mechanical properties of laser spot welded joints of dissimilar metals as a novel method for joining thin sheet material in SynRM rotors. The materials being examined are thin sheets of Stainless Steel 316L and Mild Steel 340LA. The intended research focuses on the surface smoothness of laser welded joints, tensile-shear analysis and weld cross-sectional evaluation of spot welds using an optical microscope and laser profilometer. Additionally, the study incorporates the DOE and statistical analysis of results by applying the Taguchi method.

2 Literature Review

In this section, applications, current construction methods and the possible drawbacks of SynRM motors are briefly discussed. Then laser welding and its application in electrical vehicle applications is explored and laser spot welding as a modern method to apply in electrical motors is introduced.

2.1 Synchronous Reluctance Motors?

Synchronous reluctance motor is an electric motor that operates based on the natural tendency of magnetic flux to follow the path of least resistance, known as magnetic reluctance, within the motor's rotor.

SynRMs do not have permanent magnets or windings (on the rotor side). This characteristic distinguishes SynRMs from other kinds of motors, including permanent magnet (PM) motors and induction motors (IM). Instead, torque is developed through the rotor's tendency to align itself to the magnetic field to minimize magnetic reluctance, which hinders magnetic flux. This allows SynRMs to achieve high efficiency with cheaper and simpler rotor structures

The remarkable benefit of SynRMs is that no rare-earths material is involved in manufacturing one, making them environmentally and economically suitable for Electrical Vehicles (EV) and industries. Rare-earth materials, such as neodymium involved in the construction of permanent magnet motors, are expensive and sensitive to supply chain issues. SynRMs bypass these constraints by using materials such as laminated steel, reducing manufacturing cost and keeping efficiency comparable, especially for applications that need high speed and dynamic performance, as they could operate in smaller sizes and lower moment of Inertia for the same power output. Due to lack of PMs in the rotor structure and lower temperature in bearing and winding, SynRM is more reliable and requires less maintenance compared to conventional motors. Due to the capability to operate in cooler temperature, SynRMs obtain more efficiency within the same power range and frame size, as well as higher power density and torque per ampere relative to Ims. (Taghavi & Pillay, 2014, p. 330.)

Figure 2 illustrates the structure of rotor that is manufactured by segments and barriers in a Synchronous Reluctance Motor.



Figure 2. structure of Rotor in SynRMs (Taghavi & Pillay, 2014, p. 330).

2.1.1 Application of Synchronous Reluctance Motors

SynRMs are becoming very vital in various industrial and automotive applications due to their relatively good efficiency, low cost, and absence of rare-earth materials. Electric traction systems are among the main applications that use SynRMs, mainly for EVs, where high torque and power density is highly critical along with fast dynamic response and wide operational range in speed coverage. Compared to PMSMs and IMs, SynRMs have lower cost with reduced rotor losses. Thus, they are a good candidate for electric powertrains. Other than automotive traction, SynRMs are applied in industrial applications of pumps, fans, compressors, etc., since their dynamic response and reliability are excellent. Improvements in rotor geometry and control strategies have optimized their performance to meet the requirements, hence making the machines competitive in automotive and industrial fields.

(Heidari, Rassölkin, Kallaste, Vaimann, Andriushchenko, Belahcen & Lukichev, 2021, p. 2.)

Figure 3 summarizes the different features of the dominant motors and SynRMs.





Motor Type	Stator and Rotor Structure Sample	Different Types	Main Applications	Superiorities	Drawback(s)
IM		<ul style="list-style-type: none"> • copper rotor • aluminum rotor • wound rotor • rotor skewing 	Industrial applications (pump, fan, traction, etc.)	<ul style="list-style-type: none"> + low cost of material and manufacturing process + line-start capability 	<ul style="list-style-type: none"> – low power factor – highly probable bearing fault
PMSM		<ul style="list-style-type: none"> • interior PM [42] • surface-mounted PM [43] • line-start PMSM 	precise control and high-speed performance (traction, robotics, aerospace, medical, etc.)	<ul style="list-style-type: none"> + high performance in wide speed range operation 	<ul style="list-style-type: none"> – rare-earth material usage
SynRM		<ul style="list-style-type: none"> • line-start SynRM • skewed rotor • rotor with asymmetric flux barriers 	Industrial applications (pump, fan, traction, etc.)	<ul style="list-style-type: none"> + reliable and highly efficient due to cold rotor operation + high dynamic + high overloadability + very high-speed capability 	<ul style="list-style-type: none"> – high torque ripple – severe low power factor
PMSynRM		<ul style="list-style-type: none"> • rotor skewing • asymmetric rotor structure • different barrier structure and PM material 	Traction applications	<ul style="list-style-type: none"> + very high performance without rare-earth PMs 	<ul style="list-style-type: none"> – hard manufacturing and installment process

Figure 3 Comparison of motor technologies (Heidari et al., 2021, p. 3).

Applications involving in-wheel motors, especially in electric vehicles, are an up-and-coming outlet for SynRMs. In recent years, a hybrid motor design consisting of a PM Assisted SynRMs has been used in these systems to exploit the advantages of PM and SynRMs such as low cost, low PM composition, high torque density, and high efficiency. In an in-wheel configuration, the motor is directly integrated into the wheel, thus eliminating complex mechanical transmissions and differentials. This, in turn, allows it to be more efficient and compact. SynRMs, especially those of external rotors, offer better torque control and reliability. Besides, the high dynamic performance with the fault tolerance of these motors serves for traction control and handling improvement of the vehicle for better drive. (Bonthu, Arafat & Choi, 2017, pp. 1–2.)

2.1.2 Construction Methods for Rotors

Several novel construction methods are utilized to improve the efficiency, durability and performance of SynRMs' rotors. For instance, recent advancements in rotor design, such as skewed or asymmetric rotor flux barriers, have helped improve in the SynRMs' performance by reducing torque ripple and enhancing dynamic response, making them an optimistic selection in high-performance industrial applications. (Heidari et al., 2021, p. 3.)

Asymmetric flux barriers, which are non-magnetic slots in SynRMs, are designed asymmetrically within the rotor to guide magnetic flux along optimal paths, minimize torque ripples, and thereby enhance overall efficiency. The laminations with angled positions in skewed rotors, concerning an axis reduce torque pulsations, lowering acoustic noise and, hence offering much smoother operations. However, the complexity of aligning and integrating the rotor structure negatively affects the manufacturing and installation process. However, the complexity to align and integrate the rotor structure negatively affects the manufacturing and installation process. (Chai & Dong, 2024, pp. 360–361.)

The axially laminated anisotropic (ALA) rotor is a type of rotor in SynRM that includes a rotor made of alternating layers of magnetic and non-magnetic materials, making the rotor highly anisotropic and optimizing its performance for high-speed applications. By optimization of magnetic and non-magnetic material arrangements, this construction method reduces the formation of rotor eddy current losses, ensuring higher efficiency. Specific processes are required to manufacture these rotors to ensure robustness, such as hot isostatic pressing, vacuum brazing or explosion welding. These methods improve the functionality and robustness of the rotors, but they also have some drawbacks such as torque ripple. Multi layered SynRMs arrangement aimed at using multiple layers to achieve better flux control, mitigating eddy current losses, while increasing the efficiency of motors, particularly in high-speed applications. The laminated structure enables better control on the torque ripple, ensuring a smoother functioning of the motor with higher reliability. Hot isostatics pressing is a technique to manufacture rotor layers. While the layered structure offers advantages in performance, ensuring adequate mechanical strength the formation of thermal stresses between layers adds complexity to manufacturing processes. (Abramenko, Nerg, Petrov & Pyrhönen, 2020, pp. 117377–117387.)

Additionally, the design of multiple disks can play a key role in the mechanical performance of EVs, as it distributes the mechanical stresses more uniformly throughout the disk leading to a reduction of the occurrence of material failure under high-stress and dynamic loading conditions. It ensures that the motor can work under a higher functional load without losing its structural integrity. (Gerlach, Zajonc & Ponick, 2021, pp. 97–98.)

The manufacturing process and assembly of multi-layered rotors for synchronous reluctance motors include different methods such as clamping, riveting, welding, stamping, and bonding. (Ziegler, Brandl, Kuehl & Franke, 2021, p. 2.)

Arc welding has long been applied on the surface of the motor stack where the magnetic flux is relatively low. However, it might lead to a significant share of the core material that does not conduct magnetic flux. Therefore, the core that is welded was designed to have extra-large dimensions to compensate for the damaged material by the welding, to make it suitable for industrial applications.

The most common and effective techniques are stamping and lamination which enhance the desired mechanical integrity and electrical performance. Stamping means cutting off the individual sheets from the magnetic material with high quality and precision. The next step, lamination, is to assemble and stack the thin layers over each other, applying an adhesive material such as Epoxy resin between each layer to improve the integrity of the structure. The lamination process is finalized with the hot-pressing procedure or cooked in a furnace for the resin to set in. (Taghavi & Pillay, 2016, pp. 3370–3371.)

Ribs are designed and added to the rotors' sheet structure to improve the mechanical strength of the sheets, increasing the reliability of SynRMs while spinning at high speed, and withstanding centrifugal force (Figure 4). (Dziechciarz, Oprea & Martis, 2016, p. 1709.)

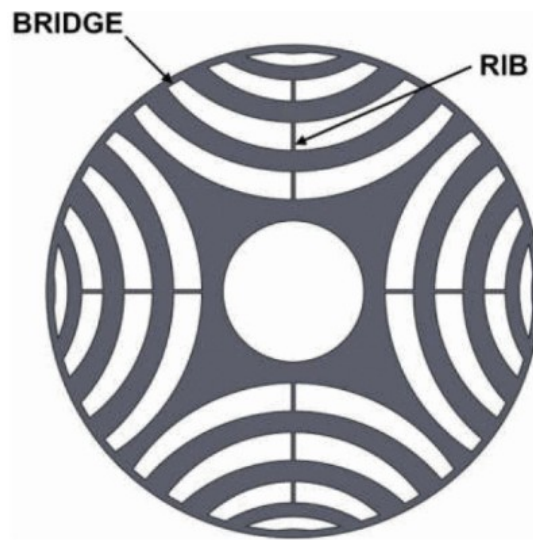


Figure 4. SynRM rotors geometry-ribs (Dziechciarz et al., 2016, p. 1705).

Although thicker ribs provide better mechanical strength, it impacts negatively on the power factor by increasing the leakage of magnetic flux. (Kim, Park., Oh, Jang, Won, Chun & Lee, 2020, p. 15.)

Additionally, the effect of manufacturing stresses observed during cutting, close to the machined edge of the rotor core, resulting in mitigating permeability and negative effect on motor's efficiency. (Credo, Petrov, Pyrhönen & Villani, 2022, p. 1253.)

The layers have iron tips and bridges to further ensure the mechanical integrity of rotors. In high-speed and high-power applications of SynRMs, to endure high centrifugal force, these bridges must be even thicker. However, these bridges also considerably decrease the electromagnetic performance of motors and create leakage flux and in some cases saturation of magnetic flux causing overheating. The purpose of a Bridgeless Rotor (BLR) for SynRMs is to develop electromagnetic performance and improve torque and power factor by removing the tangential and radial bridges. One way to eliminate these bridges (Figure 5) is to utilize adhesive materials such as glue to join the magnetic flux guideways. However, due to elevated temperatures during operation, the mechanical properties of glue can weaken, leading to the failure of the rotor. To overcome this challenge, laser welding is used to manufacture such bridgeless motor laminates. (Allahyari, Petrov, Pyrhönen, Aarniovuori, Lindh & Parviainen, 2024, pp. 65826–65828.)

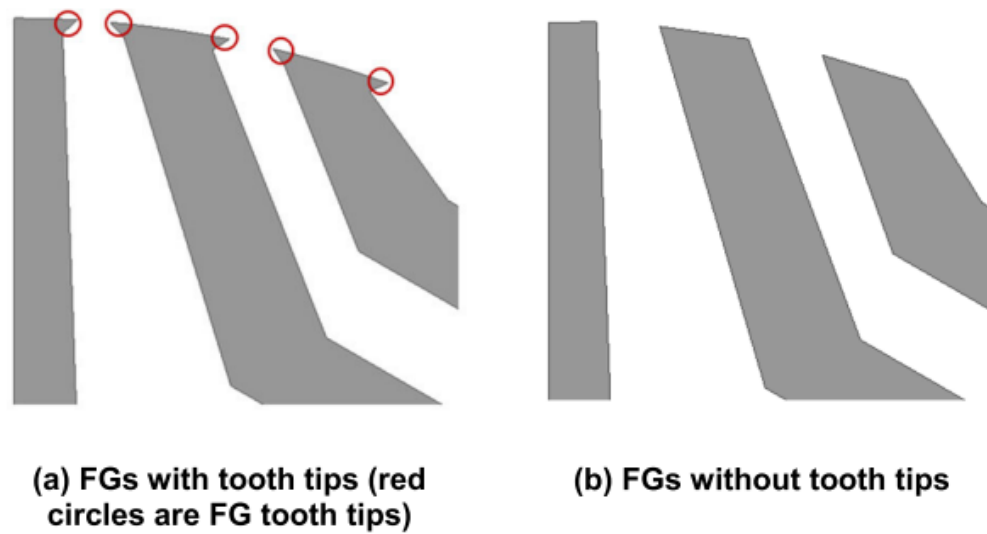


Figure 5. Introduction of Flux guides (FGs) with(a) and w/o (b) tooth tips (Allahyari et al., 2024, p. 65828).

Extensive studies and research have been conducted in this field to optimize the design of electrical motor components and develop manufacturing methods that ensure performance and efficiency. The study being conducted at LUT is proposed to remove the tangential and radial bridges from the thin ferromagnetic sheets of rotors and utilizing a non-ferromagnetic back plate (stainless steel) in axial direction to hold these flux guides in place by laser welding (Figure 6). This Thesis explores the mechanical properties and surface smoothness of welded thin sheets of rotors employing laser spot welding.

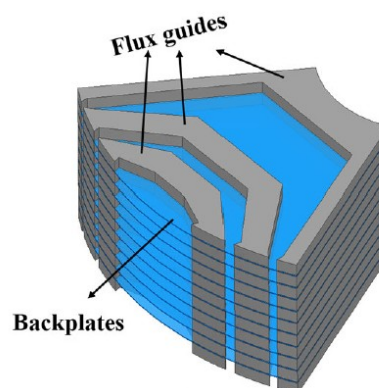


Figure 6. 3D view of proposed Bridges Less Rotor with flux guid and back plates (Allahyari et al., 2024, p. 65829).

2.2 Laser Welding

Laser welding is an advanced joining method quite commonly used in mass production systems, due to its high energy density to join various similar and dissimilar materials at high speeds and significant precision with minimal distortion.

Traditional welding methods usually apply extreme heat with a large thermal impact, which results in the generation of high thermal stresses and distortions, especially in thin materials. Laser welding employs a focused and concentrated beam which enables performing intricate welds more efficiently and with fewer imperfections, which is crucial for joining complex geometries and hard-to-weld materials. Moreover, for applications that require deep penetration or narrow welds, laser welding is a highly effective technique. In deep penetration welding, a keyhole is formed due to the implementation of high power density that vaporizes the surface of the material at the focal point. The keyhole allows the laser beam to penetrate deeper through the material with narrow HAZ, leading to a high depth-to-width ratio. (Ai , Jiang, Wang, Mi and Geng, 2018, pp. 779–789.)

Figure 7 shows the power density, bead geometry and penetration of laser welding compared to the electron beam (EB), plasma and arc welding. The higher penetrations of EB are achieved in lower welding speed and in the vacuum conditions.

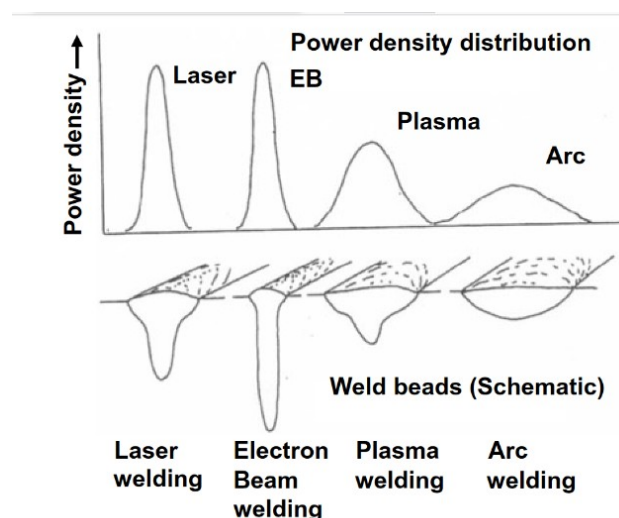


Figure 7. Power density profiles and weld bead geometries of Laser, EB, Plasma and Arc welding (Katayama, 2020, p. 36).

The heat-affected zone (HAZ) observed in laser welding is narrow compared to traditional welding methods. This helps in mitigating material degradation and structural failure around the weld and ensures the structural and metallurgical integrity of the components. It is based on a non-contact nature, resulting in minimum wear and tear of the tools, making this method more suitable for large-scale production and industries.

2.2.1 Laser beam shapes

In order to control the morphology and characteristics of the weld seam made by laser beam, it is imperative to control the power distribution of the beam itself, laser beam shaping is basically how to control and utilize the intensity distribution of laser beams for a specific optical performance based on geometrical optic principals. (Shealy, 2000, p. 1.) Solidification rate and processing efficiency in laser-related manufacturing methods are directly influenced by various beam shapes (Seibold, Schrickler, Schmidt, Diegel, Friedmann, Hellwig, Fröhlich, Nagel, Kallage, Rack, Requardt, Chen & Bergmann, 2024, pp. 1–2). According to Bremer, Aarts & Römer (2024, p. 1), the thermal field generated by the local laser and subsequently their local thermal gradient and thermal cycles are significantly affected by power distribution of laser beam shape.

Lasers that are utilized in different industries for actual materials processing are known by characteristics of their emitted medium or materials, oscillation medium, shapes, pulse width, and wavelength, and classified into solid, liquid, and gas lasers. For instance, CO₂ laser, as a gas laser, has long wavelength. This laser is emitted during the transition from upper to lower energy level from asymmetric stretching vibration. High power pulsed wave CO₂ laser is utilized in drilling, while continuous wave are mostly employed for cutting and welding. However, swelding of thin sheets of steels are mainly performed by fiber lasers or disk lasers in place of CO₂ laser in recent years. (Katayama, 2020, pp. 5-8.)

In fiber laser, however, the gain medium is an optical fiber (such as high-purity Silica), doped with a rare earth element such as Yb³⁺. The laser beam is efficiently emitted by laser diode pumping. The power of fiber laser can be increased by utilizing a beam combiner to merge laser beams from fiber-delivered modules, making this technique suitable for achieving higher power, intensity, and efficiency. High beam quality, lightweight and compact size, and long-distance beam delivery through fiber are the other advantages of this laser

technology. Single mode fiber laser provides high quality, narrow and well-focused beam, making it suitable for micro processing, and precise welding and cutting, whereas multimode fiber laser has a broader beam, and a longer delivery distance, making it ideal for heavy-duty industrial processing applications, for instance, shipbuilding. (Katayama, 2020, pp. 13-14.)

2.2.2 Core and Ring-shape Laser welding

The ring-shaped laser beam is one beam shaping technology, which has been found to have high development potential for improved keyhole-mode laser welding. Laser welding process is commonly performed using multimode beam. This has often brought along defects like spatter formation due to an unstable process of keyhole behavior. Immature spatters may destroy not only the appearance but also the structural quality of welds, particularly in high-reflect materials. A superimposed ring-shaped beam introduces novelty in the way it redistributes laser energy around the keyhole, giving stability to the latter with an enlarged entrance. The violent metal flow responsible for spatter occurrence is reduced, leading to an improved smoothness of the weld surface. In fact, a ring-shaped beam will help fabricate a smooth weld surface and improve the weld performance. A superimposed core and ring-shaped (SCR) beams can develop finer control of the thermal-fluid dynamics inside the molten pool, which in turn leads to less mass loss and fewer imperfections in the weld. The present technology has wide applications in industries operating under highly precise welding requirements, such as in aerospace, automotive, and shipbuilding, where technology can be applied to provide more reliable and expedient methods for producing welds with minimal defects. (Wang, Jiang, Chen, Du, Lei, Zhao & Chen, 2024, pp. 1–3.)

Figure 8, illustrate a diagrammatical sketch set up of SCR laser welding for a 2 in 1 Fiber laser which guides the beam transmission in the core and ring fiber individually.

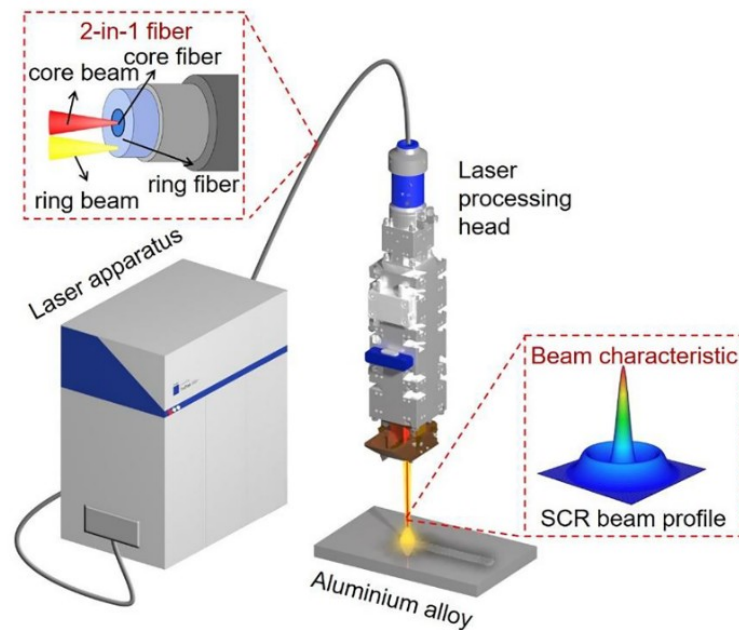


Figure 8. diagrammatical sketch set up for SCR Laser Welding (Wang et al., 2024, p. 2).

2.2.3 Laser Welding in electrical motors

When using welding as a method to attach the laminated steel parts of electrical motors, the morphology and characteristics of the weld bead have a significant effect on the magnetic and mechanical properties of the rotors. In some cases, the thermal stress caused by weld beads can lead to a reduction in magnetic efficiency and increase iron loss that is the energy lost in the form of heat within the iron core of electrical machines. However, by optimizing certain parameters and exploring novel strategies, such as shaping the laser beam, a more stabilized molten pool, and smoother surface can be achieved, reducing the molten-pool fluctuation in the surface of laminated electrical steel sheets. (Tang, Zhang, Wan, Ouyang, Gao, Wei, Wang, Yang, Wu & Zhang, 2023, pp. 1–2.)

The state of arts shows that laser welding positively impacts the joining of thin laminations in electrical motors. Laser technology can provide significant advantages as compared to arc welding for stacking thin sheets, as it allows for high-quality welding of thinner sheets (up to 0.2 mm) and thicker insulation layers ($>1.5 \mu\text{m}$). (Ziegler, Mayr, Seefried, Kuehl &

Franke, 2019, p. 2.) Furthermore, the quality of the process could be monitored to optimize the parameters, allowing real-time adaptation to changing conditions. With laser welding technology, working with thin, high alloyed sheets is possible, and it is also feasible to adjust the weld seam cross-section and the heat input zone. However, irregularity and defect may still occur in the welded seam (Ziegler et al., 2019, pp. 2–4.)

Laser welding significantly affects the performance of electrical steel laminations, especially in high-speed electrical machines. The main drawbacks associated with this technique include the generation of short circuits between laminations and mechanical stress due to thermal expansion during axial welding of stacked layer and without any supporting sheets. These effects lead to increased eddy currents and higher core losses that further degrade the overall magnetic properties and reduce efficiency. Also, the microstructural alterations in the heat-affected zones of the welded regions can further contribute to magnetic deterioration. Laser spot welding with supporting sheets can help in mitigating the challenges. It helps in the reduction of magnetic losses and provides sufficient mechanical strength to satisfy or surpass the requirements for the electrical steel to perform at a high rotational speed with minimal performance loss. (Zhang, Tang, Di, Wang, Wu & Wang, 2024, pp. 1–8.)

The process steps for manufacturing thin layers of electrical motors include cutting, stacking and joining of laminations. Joining electrical steel thin laminations is highly dependent on an optimum balance between the electromagnetic characteristics and mechanical strength based on application. The automated process of joining very thin sheets by laser welding allows for high-strength products with low distortion. Products with welding of low-alloyed steel are also possible. For high-frequency applications, spot welds between the sheets can reduce losses. (Ziegler et al., 2021, p. 2.)

2.2.4 Laser Spot Welding

Laser spot welding (LSW) is mostly concentrated on creating discrete, high precision welds in localized areas. It is valuable for applications that require precise control over bead size, heat input, material deformation, and distortion. This subset of laser welding operates by focusing the laser beam on a small area of the material with intensive and controlled energy input, leading to localized weld formation. After applying high energy, molten material cools

down, it solidifies making a strong weld, while the rapid heating and cooling time minimizes the amount of heat distributed into surrounding material, reducing HAZ and eliminating damage to the nearby components and material warping. (Li, Mu, Luo, Huang & Pang, 2021, p. 1.)

Moreover, laser spot welding allows the joining of dissimilar materials which may have different physical and chemical properties. These types of materials are very challenging to weld with traditional welding methods. Laser spot welding controls heat input precisely, minimizing the negative effects of joining dissimilar material such as the formation of brittle intermetallic compounds (IMCs), which is a major reason for weakening the strength of welded joints, hence increasing the overall durability of welded parts. The process utilizes high energy concentration to prevent unnecessary heat distribution, allowing efficient melting of materials, making it notably beneficial for materials that have different melting points. The rapid solidification as mentioned, significantly mitigates the effects of thermal expansion and possibility of residual stress and cracks during the process. (Kuryntsev, 2021, p. 3.)

The welds provided by laser spot welding are of good quality, ensuring high strengths and fewer porosities, which are important for applications where the integrity of structures is critical, and components are faced with thermal fluctuations and high vibration and pressure. Therefore, reliable welds make this technique an excellent option for high-performance functions. Laser spot welding offers a flexible alternative for other spot weld techniques such as resistance spot welding, providing an advantage of low distortion while focussed heat source and requires only “line-of-sight (with one side of the area to be welded) fabrication”, which is a remarkable benefit for reach to more tough to access positions. Additional innovations, such as the remote welding method, can provide an even greater output rate, which is crucial where high volumes and quantities of welds associated with the manufacturing process are required. (Martinson, Daneshpour, Koçak, Riekehr & Staron, 2009, p. 3352.)

Residual stresses in laser spot welding of steel sheets are distributed between tensile and compressive areas. Though tensile stresses may be concentrated in the welding area, generally stresses inside the surrounding zones are predominantly compressive. That is the important difference from RSW, because in LSW higher tensile residual stresses are developed usually in the welded zone. However, this tensile zone in LSW is enveloped by a

larger and more significant compressive region. Since this compressive region would help to prevent crack propagation, it enhances the fatigue resistance of the weld. That is, it is more difficult for a crack to propagate since compressive stresses effectively "close" any crack tips, thereby raising fatigue life significantly in the welded structure. The specific geometry of the welding path in LSW plays also an essential role in shaping residual stress distribution. Such geometrical variations allow better control of the residual stress patterns and can improve the overall mechanical performance of the welds. Laser spot welding in steel sheets creates a favorable residual stress distribution. Such a combination of tensile and compressive stress within LSW, along with the influence of the geometry of welding, allows further opportunities for a more advantageous technique in ensuring fatigue durability for structural applications. (Martinson et al., 2009, pp. 3355-3357.)

A study by (Leuning, Steentjes, Hameyer, Gerhards & Reisgen, 2017) explored the laser spot welding method and traditional linear welding to join the electrical steel laminations (around the stacked lamination) in rotating electrical machines (Figure 9).

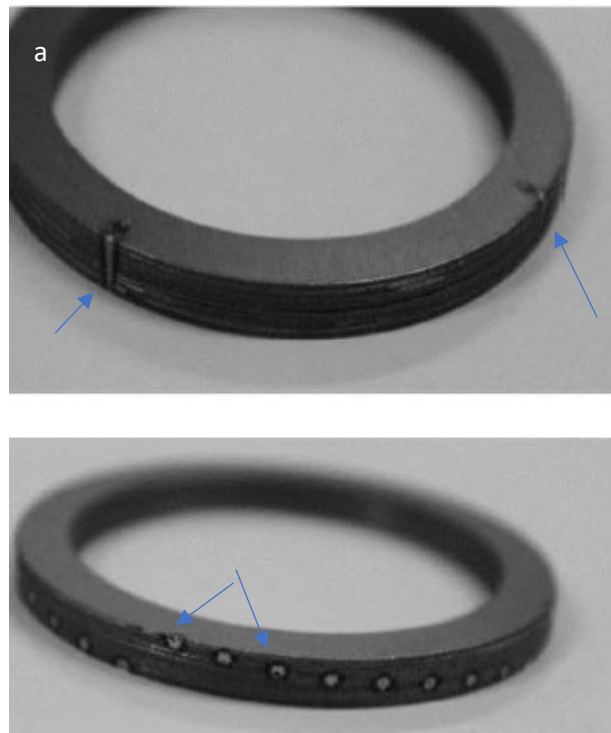


Figure 9. Welding joint (a) Linear welding line (b) Laser Spot Welding (Leuning et al., 2017, p. 2).

The result showed that LSW has a positive impact on the magnetic properties, especially at high frequencies. The spot-welding method limits the area of deterioration, while in linear welding, with greater magnetic loss and increased coercivity, the area of affected material is greater. Therefore utilizing LSW, mitigates eddy current paths, which causes losses at high frequencies, and allows for a more controlled microstructural change. The study, therefore, concludes that although the spot method of welding is promising, especially in high-frequency applications, further refinements of laser parameters and controlling the stresses are needed to exploit its benefit relative to magnetic and mechanical performance fully. (Leuning et al., 2017, pp. 1–3.)

Based on the above literature review pertaining to the laser spot welds, it is deemed necessary to investigate this strategy further as there aren't many studies that discuss the mechanical and morphological properties of the spot welds to ensure robust construction of novel electrical machines. In the subsequent section, materials and methods used in this experimental study are introduced.

3 Materials and Methods

In the field of Electrical Vehicles (EVs), the manufacturing of Synchronous Reluctance motor rotor layers and the method of attaching the layers play significant roles in their performance and durability. This chapter introduces materials and methods utilized to evaluate and characterize the objective of the thesis. Additionally, the practical work conducted on these parameters is discussed.

3.1 Materials

This thesis explores the assembly of three thin sheets (a combination of magnetic and nonmagnetic) used in a rotor module. The sheets comprise a thin 0.25mm Stainless Steel (SS 316L) sandwiched between two 1mm-thick sheets of SSAB Domex 340LA steel. These three sheets were joined together using laser spot welding. (Figure 10)

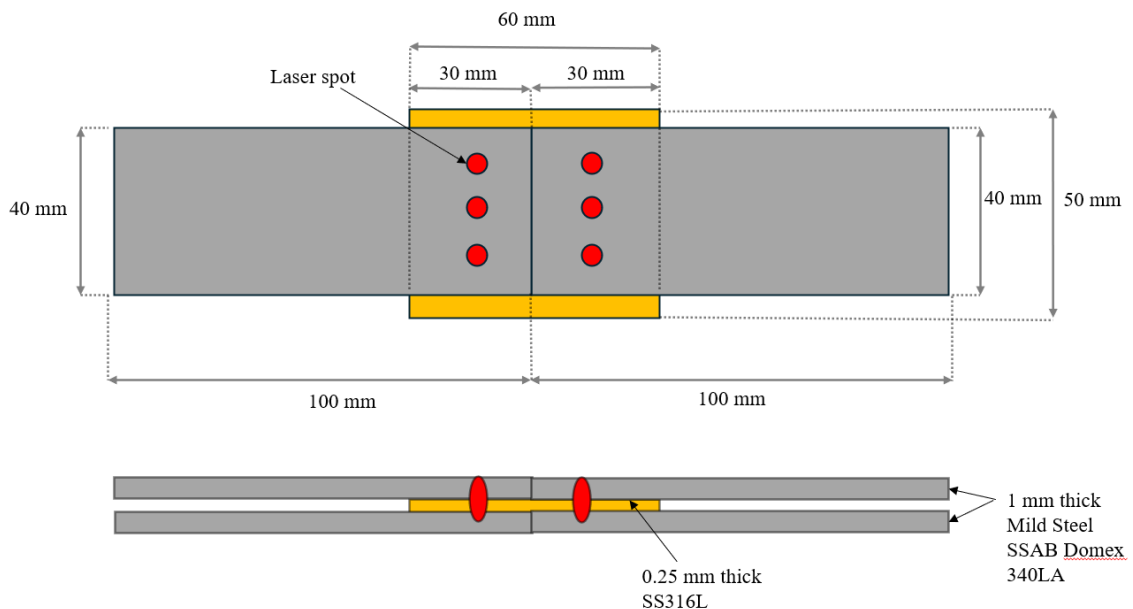


Figure 10. Dimension and figure of the test specimen

The dimensions of SS 316L were $60 \times 50 \times 0.25$ mm, and those of Mild Steel (MS) 340LA were $100 \times 40 \times 1$ mm. Stainless Steel (SS) 316L has a low carbon content that mitigates the possibility of corrosion. It has superior corrosion resistance following welding or stress relieving, making it suitable for demanding environments. It exhibits high creep strength at elevated temperatures.

Stainless steel 316L is hardened with a mixture of grain size and precipitation refinement, leading to high strength with low alloy content and this ensures excellent weldability without softening in the weld zone or any coarse-grain formation. They are especially suitable for structural components. Because of their corresponding yield strength levels, SS 316L all reveal low-temperature brittle fracture strength and remarkable cold forming, hence ideal for cost-effective solutions in parts and sub-assemblies where size, thickness, and weight reduction are required. The SS 316L has normally an austenitic structure which is non-magnetic and corrosion resistant. However, the cold rolling process can change some austenitic into martensite with ferritic properties. Therefore, in this study, annealed SS 316L has been used to ensure austenitic microstructure and to retain the desirable mechanical properties. The actual thin discs intended to be joined in a SynRM rotor are demonstrated in Figure 11.

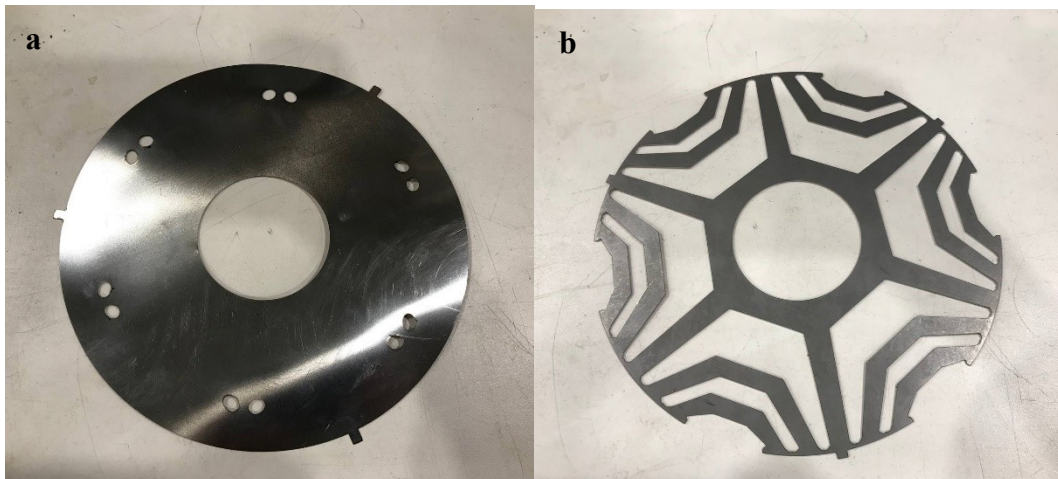


Figure 6. Actual rotor layers of SynRM, (a) SS (b) MS thin sheets

3.2 Experimental methods

This section introduces systems and methods. The systems and methods are utilized to implement, measure, and evaluate experimental work.

3.2.1 Laser System

Laser spot welding, especially when working with materials that need high accuracy and low distortion, requires high precision in energy delivery and beam focus. Therefore, an advanced laser system was employed in this study. A 6kW TRUMPF (Figure 12) double fiber laser coupled to programmable focusing PFO33 optics was utilized during the welding process.



Figure 12. TRUMPF 6KW Fiber Laser

Table 1 describes the specification of laser sources used for the experimental study.

Table 1. Laser source specification

Parameters	Levels
Wavelength (λ)	1070 nm
Core Diameter (d_c)	25 microns
Ring Diameter (d_r)	100 microns
Focal length (f)	450 mm
Core spot size (ϕ_c)	71 microns
Ring spot size (ϕ_r)	337 microns
Max power in Core (P_c)	2kW
Max power in Ring (P_r)	4kW

It is worth mentioning that the minimum power in the laser system for core power is 80 W and for ring power is 40W.

3.2.2 Optical Microscope

To observe and examine weld morphology, optical microscopy provides insight into how welding is affected by various parameters. In this thesis, the device was used to evaluate spot welds cross-section and capturing images. The optical microscope utilized was WILD model M400 in conjunction with camera XCAM model 1080P and is shown in Figure 13.



Figure 7. Optical microscopy -WILD M400

3.2.3 Laser Profilometer

One aim of this study was to achieve a high-quality weld with the minimum protrusion on the weld surface. To measure and inspect the LSW profile, a laser profilometer was used. The device utilizes laser scanning to provide a detailed 3D profile of the weld and create specific information about the topology and flatness of the specimen surface. Profilometer model Keyence VR-3200 1104 (Figure 14), was used for this study.

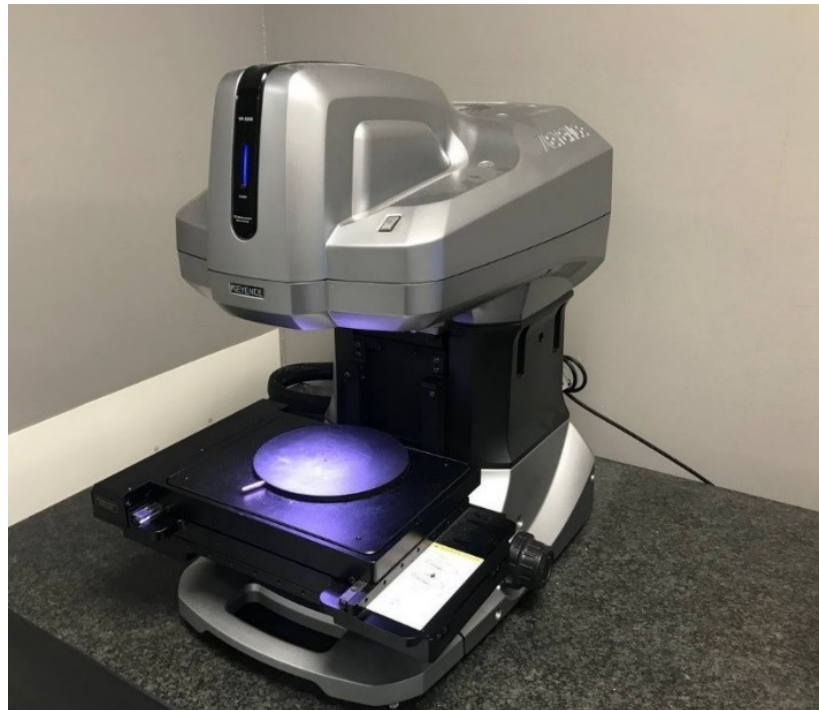


Figure 14. Profilometer-Keyence VR-3200 1104

3.2.4 Tensile Test

The other objective of this thesis is to evaluate the maximum force needed to achieve maximum tensile strength of laser spot welded thin layers. The tensile testing machine was utilized for this purpose.

In this thesis, a tensile test machine Model Zwick/Roell Z0201 (Figure 15) was used in conjunction with testXpert III software to conduct the tests and gain numerical results.



Figure 15. Tensile test machine-Model Zwick/Roell Z020

4 Experiments

This chapter covers all the experimental procedures that were conducted in this study. First, a preliminary evaluation was conducted to determine the optimum power range and laser beam interaction time needed for sufficient penetration, followed by welding the specimens for tensile testing. Once the test requirements were met, more samples were provided. The spot weld protrusion for all different parameters was measured and the cross section of spots was prepared, measured and evaluated.

4.1 Preliminary Studies

The first step to start laser spot welding of defined layered material was to evaluate at what stage the penetration accrues through the thin sheets. Since laser spot welding was utilized, the variable parameters considered were core power, ring power, and interaction time, and focal plane was kept on plate surface.

To fine-tune the parameters, smaller circular pieces (65Ø mm) of MS and SS were prepared allowing for quicker penetration assessments with less material usage. The following sections present a detailed overview of the steps and results.

4.1.1 First run

In the first welding run, laser spots on one sheet of Mild Steel were performed (Figure 16). The experimental campaign started with making laser spot welds on a single sheet of MS. Aim was to achieve full penetration in the MS sheet.

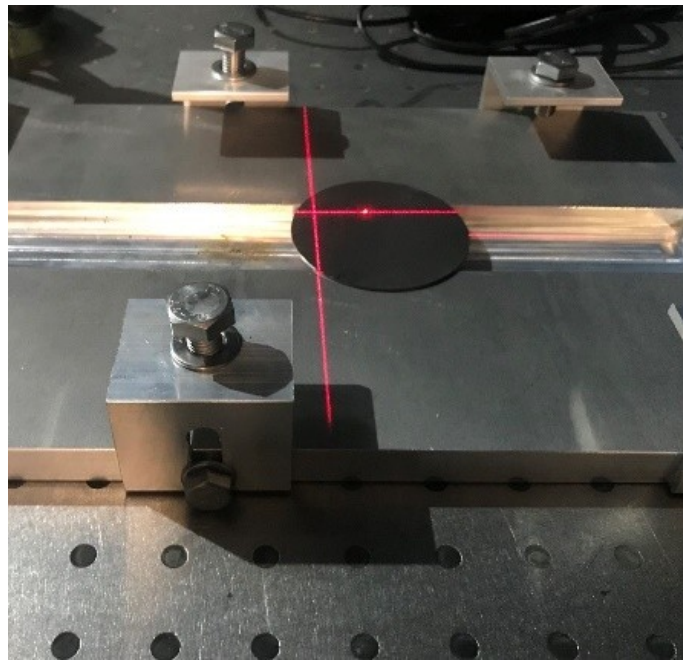


Figure 16. First setting for Mild Steel

Based on previous studies done at LUT, five different beam interaction times and three levels of core and ring power were selected. The results are shown in Figure 17. It was observed that penetration occurred at all parameters.

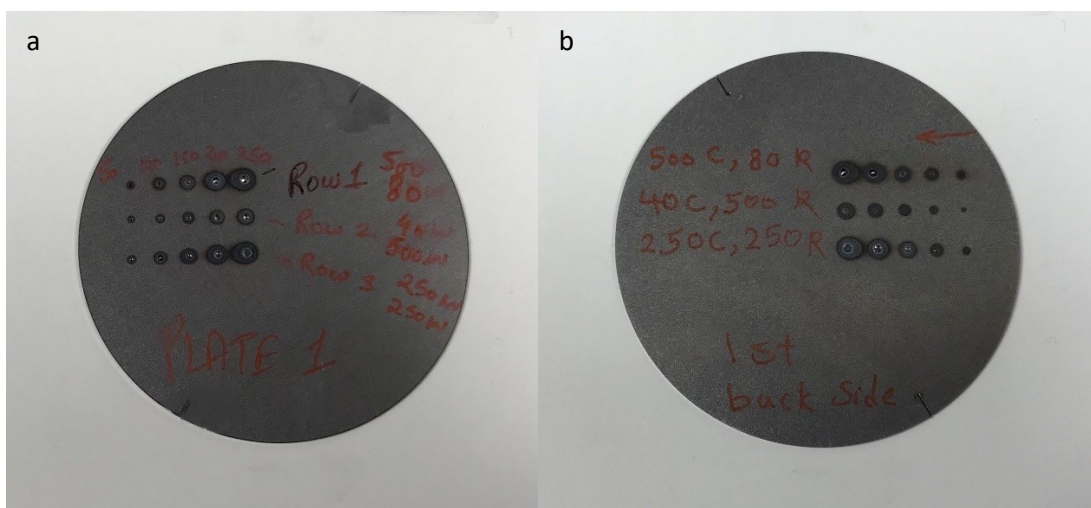


Figure 17. First Run welding Results (a)front side (b) back side

4.1.2 Second Run

At this stage, the core and ring power increased to observe weld penetration in the MS sheet as well as to assess visual quality. Additionally, the distance between spots increased to improve visibility as shown in Figure 18.

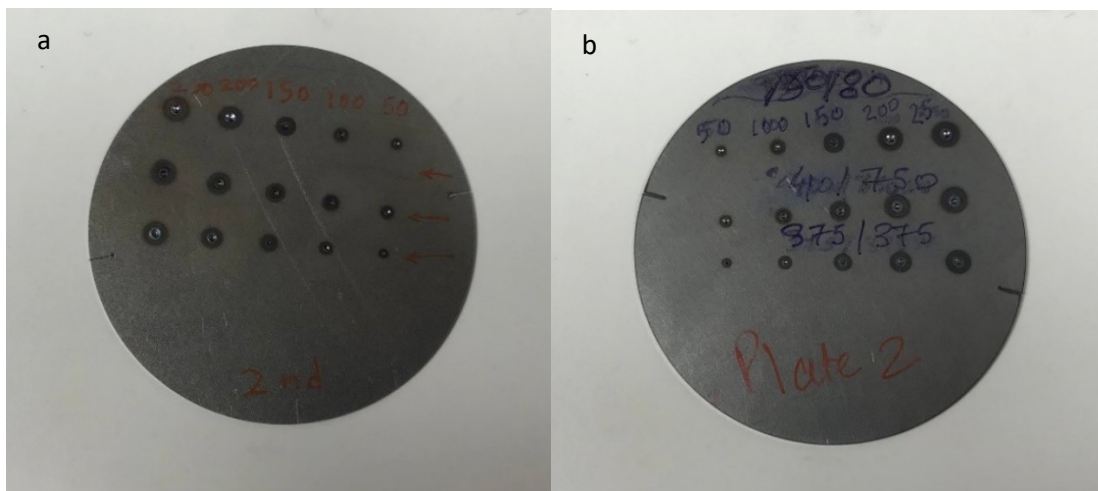


Figure 18. Second run Spot Welds on MS (a)front side (b) back side

In the second run, penetration was achieved, however, the weld protrusion height and affected zone were larger at 200 and 250 milliseconds.

4.1.3 Third Run

In the third phase, the core and ring power were increased, while interaction time was evaluated at the three first levels (50, 100, and 150 milliseconds) and the results are demonstrated in Figures 19a and 19b. In the first row, 1000 W core power with 80 W ring power, in the second row 1000 W ring power with 80 W core power and in the third row with 500 W core and 500 W ring power were applied.

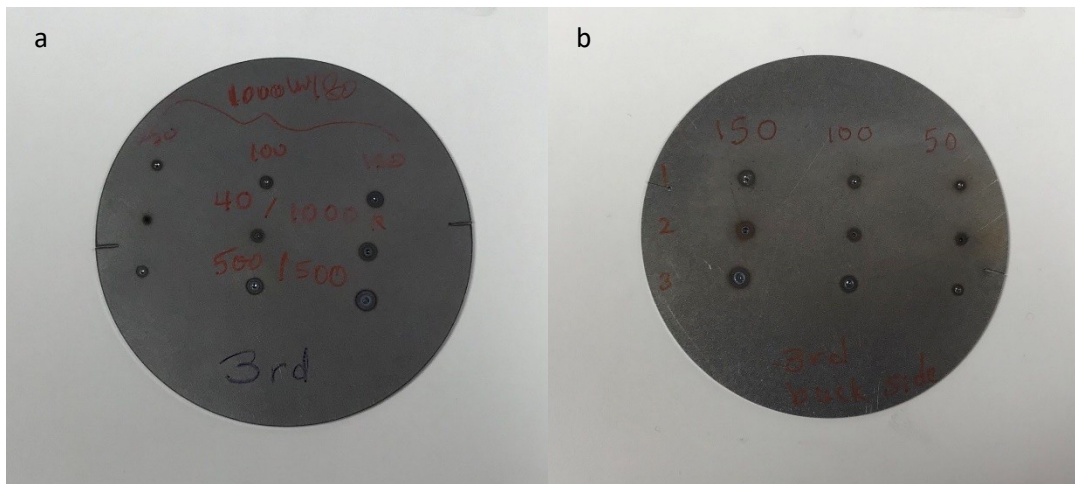


Figure 19. Third run on MS (a) front side (b) backside

The results indicated that penetration and weld quality were satisfactory, allowing the addition of the next thin layer in a subsequent step.

4.1.4 Fourth Run

In this part of the procedure, the SS sheet was added to MS to evaluate how the final power and time settings perform for two sheets. All parameters, core and ring power and interaction time, were kept constant in this run to assess the performance for the two layers (Figure 20).

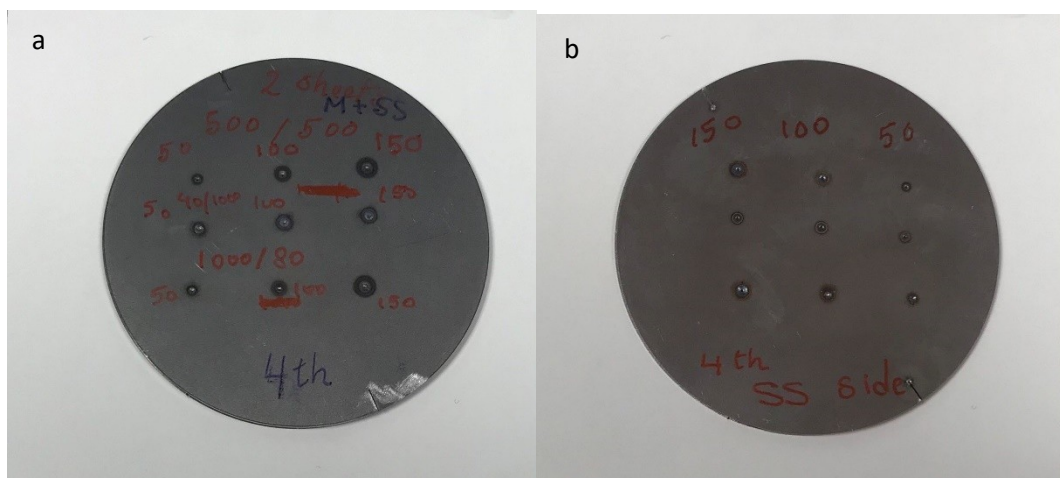


Figure 20. Fourth run on MS+SS (a) MS front side (b) SS backside

The results indicated that there was still reasonable penetration and quality, allowing the attachment of the bottom MS layer.

4.1.5 Fifth Run

In the final run at this stage of the project, two back layers of MS with one intermediate layer of SS were joined through laser spot welding while all other parameters remained unchanged. The results are illustrated in Figures 21a and 21b.

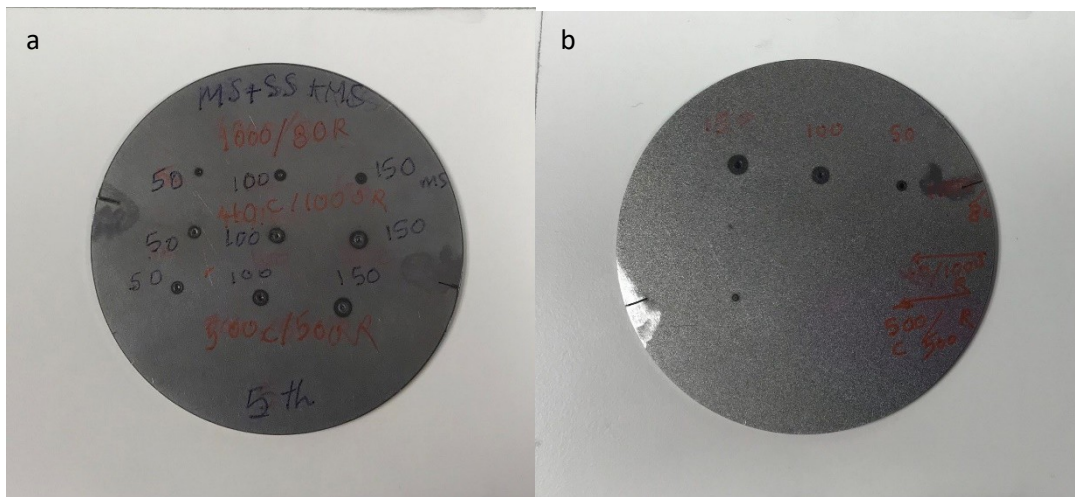


Figure 8. Fifth run on MS+SS+MS (a) first MS sheet's front side (b) third MS sheet's backside

The results indicated that there was enough penetration in the third MS layer when core power was applied. In contrast, no penetration was achieved when only ring power was employed (just a minor effect observed at 150 ms interaction time). Similar outcomes were gained while the combined 500 W core and ring power were applied, but the spot effect on the third sheet at 150 ms interaction time was slightly more pronounced.

Based on the results obtained, utilizing 1000 W core power (and 80 W ring power) provided sufficient penetration. The evaluation run in five steps is summarized in Table 2.

Table 2. Preliminary experimental steps and parameters

Experiment Steps	Material	Power (W)		Interaction Time (ms)				
		core Power	Ring Power	50	100	150	200	250
First Run	Mild Steel	500	80	✓	✓	✓	✓	✓
		40	500	✓	✓	✓	✓	✓
		250	250	✓	✓	✓	✓	✓
Second Run	Mild Steel	700	80	✓	✓	✓	✓	✓
		40	700	✓	✓	✓	✓	✓
		375	375	✓	✓	✓	✓	✓
Third Run	Mild Steel	1000	80	✓	✓	✓	✓	✓
		40	1000	✓	✓	✓	✓	✓
		500	500	✓	✓	✓	✓	✓
Fourth Run	Mild Steel + Stainless Steel	1000	80	✓	✓	✓	-	-
		40	1000	✓	✓	✓	-	-
		500	500	✓	✓	✓	-	-
Fifth Run	Mild Steel + Stainless Steel+ Mild Steel	1000	80	✓	✓	✓	-	-
		40	1000	×	×	✓	-	-
		500	500	×	×	✓	-	-

As demonstrated in Table 2, the preliminary tests were performed in five runs. Each run consisted of three power levels. The first three runs were done with five different interaction times, while the fourth and fifth runs were done with three various interaction times. The “✓” indicates that penetration is observed while “×” signifies no penetration in the specimen.

Although penetration was obtained in 1000 W laser core power in the previous steps of the experiment, significant protrusion on both the top and bottom sheets was still observed. To attain more optimized outcomes, for the next experimental steps, which involved LSW protrusion measurement, tensile test, and cross-section assessment, the core power was kept constant at 900 W. Two interaction times of 100 and 150 ms were considered, while ring power was varied in four levels.

4.2 Tests and Measurements

This part explains how the Taguchi method was used for the design of experiments. The tests and measurements in this section consist of three main evaluations. First laser scanning of weld spots, then conducting and analyzing of tensile test, and finally performing procedures to obtain the cross-sectional views of LSWs and examine welds dimensions. The following subsections clarify these steps.

4.2.1 Design of Experiments (DOE)

The Taguchi method is a statistical technique for the design of experiments to determine controllable factors, reduce variation and optimize the engineering process. In this phase of thesis work, the Taguchi method was employed for experimental design and subsequent statistical analysis, using Minitab software. The core power was kept constant and thus excluded from design.

Ring power was considered one factor and assessed at four levels and interaction time was another factor tested at two levels. Subsequently, a mixed design with 8 arrays (L8) was selected. The design of Taguchi is demonstrated in Table 3, including core power as a constant value.

Table 3. Taguchi Design of Experiment

Taguchi Array L8 ($4^1 2^1$), Factors 2, runs 8			
	Core Power (W)	Ring Power(W)	Interaction Time (ms)
1	900	100	100
2	900	100	150
3	900	200	100
4	900	200	150
5	900	400	100
6	900	400	150
7	900	600	100
8	900	600	150

Therefore, based on the DOE, sample 1 represents parameter set 1, involving 900 W core power, 100 W ring power, and 100 ms interaction time. Similarly, each subsequent sample corresponds to a specific combination of parameters according to Table 3. Subsequent experimental evaluations were conducted based on the designed parameters. Specimens were then spot welded following the parameters listed in the table.

Before welding, all the thin-sheets surfaces (MS and SS), were cleaned using metal dust remover spray to eliminate grease and contaminants. Additionally, a custom-made clamp was used to securely clamp the samples, ensuring zero gaps between the sheets during welding. Laser spot welding was performed from one side (upper sheet) of overlapped joints. To ensure the statistical reliability and accuracy of the tensile tests, three samples for each set of parameters were prepared and welded (Figure 22 a, b). Additionally, one more set of specimens was welded to characterize the cross sections of spot welds.

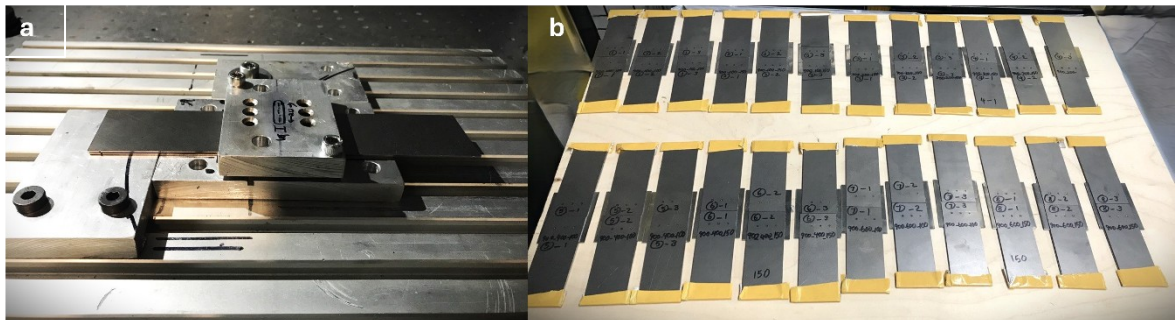


Figure22. (a) Clamping (b)Welded samples for tensile test

4.2.2 Test Execution

Since these thin modules are stacked over each other for rotor manufacturing, it is critical to have minimum spatters and weld protrusion on the surface of the weld (root and face both). This is important because an increase in protrusions and spatters leads to post-processing time, which is not suitable for mass production scenarios. Therefore, the protrusion of all spots at each test parameters level on both the front and back sides was measured systematically to increase the accuracy of the analysis. For each set of designed experiments,

twelve spots (comprising six on each side), were scanned and the maximum height for each weld spot was measured.

After scanning, a surface roughening process was applied to all test specimens to avoid slipping under the tensile force exerted by the testing machine. This was achieved using a grinding device to introduce controlled roughness on both sides of each specimen, ensuring enhanced grip and minimizing the risk of displacement during testing. Consequently, all 24 welded and prepared specimens underwent tensile testing according to ISO 6892-1:2016 and ASTM E8-16 standard, at a rate of 1,5 mm/min. Figure 23 illustrates one of the samples under the tensile test.



Figure 23. Tensile Testing

In succession, to achieve cross sections, the samples needed to be cut in small pieces around the spots, then grinded and polished to reveal cross sections of the weld spots. Subsequently, all small samples were cold moulded with acrylic resin in specific containers to make them suitable for the fine grinding and polishing machines. Finally, the test pieces were etched (Nital 4%) for microscopic evaluation.

Figure 24 (a-d) demonstrates the process used to prepare samples for characterisation. All samples were imaged utilizing an optical microscope to analyze and measure the weld

dimensions, physical attributes and internal quality. The desired dimensions were measured utilizing profilometer measurement tools.

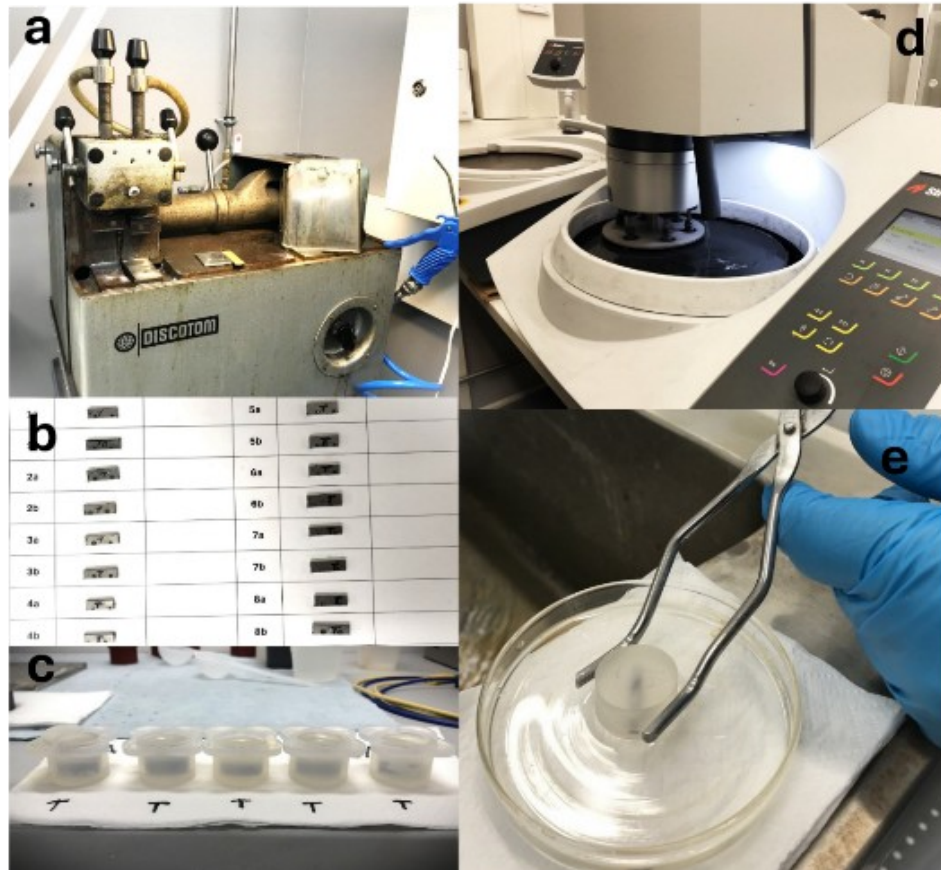


Figure 24. (a) Cutting Machine (b)Cut Samples (c) Cold Moulding (d) grinding and Polishing (e) Etching

5 Results

This portion of the study provides an overview of the outcomes of all experimental setups. The analysis is structured into three main phases: Weld spot protrusion measurement, tensile-shear test, and weld spot cross-section evaluation.

5.1 Maximum weld protrusion measurement

As outlined in the previous sections, the smooth surface of thin sheets of rotors to attain an integral component in electrical applications is of great significance. Therefore, during the laser scanning measurement utilizing a profilometer, efforts were made to identify the most critical points and measure the maximum height of each spot weld to ensure accuracy in the results. According to the design of experiments, all the weld spots for each parameter were measured individually on both sides and the results are summarized in Table 4.

Table 4. Weld spots protrusion measurement

Sample	Parameters			Top side weld spots protrusion (μm)						Back side weld spots protrusion (μm)						Avg (μm)
	Core (W)	Ring (W)	Time(ms)	1	2	3	4	5	6	1	2	3	4	5	6	
1	900	100	100	52	48	94	67	20	63	305	79	103	147	45	104	94
2	900	100	150	78	61	32	12	31	22	102	252	97	173	96	103	88
3	900	200	100	20	172	12	8	124	8	45	210	84	109	72	108	81
4	900	200	150	54	10	17	11	26	13	67	129	56	72	131	54	53
5	900	400	100	94	110	9	228	210	135	42	43	54	62	42	24	88
6	900	400	150	160	28	328	61	9	18	147	170	52	53	170	88	107
7	900	600	100	28	315	8	28	233	8	62	9	49	34	49	75	75
8	900	600	150	49	20	105	12	35	17	8	29	25	243	11	19	48

The underlined and bolded values in the spot protrusion column of Table 4 indicate the highest value for each set of parameters. However, the underlined value in the last column represents the minimum average of spot protrusion across all sets of parameters. One of the highest average weld protrusions was found in sample 1 with lowest ring power and 100ms interaction time. as displayed in Figure 25.

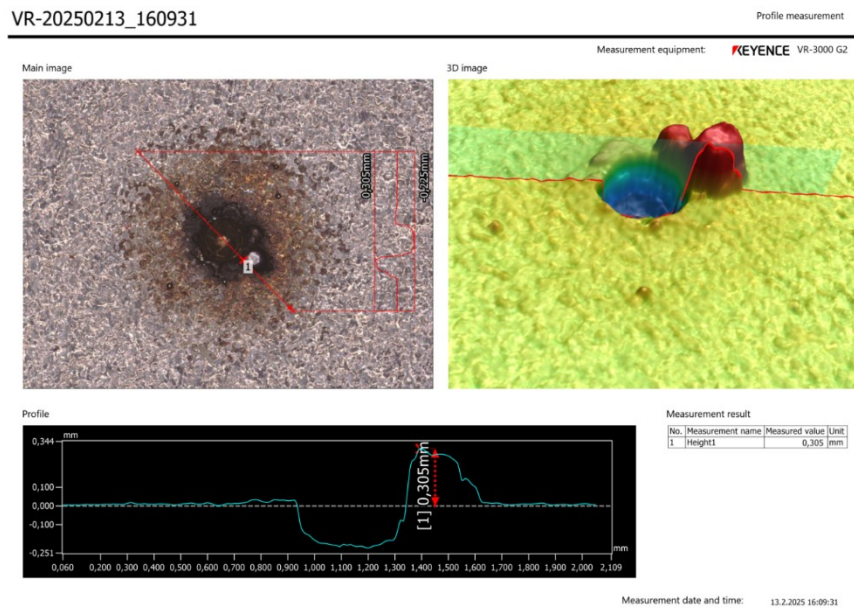


Figure 25. Weld height in the first parameter (900 W,100 W, 100 ms)

The above image shows the main spot, its 3D representation, and its profile. The maximum weld protrusion among all measurements occurred in the 6th parameter, when the ring power was 400 W and interaction time was adjusted to 150 milliseconds as demonstrated in Figure 26.

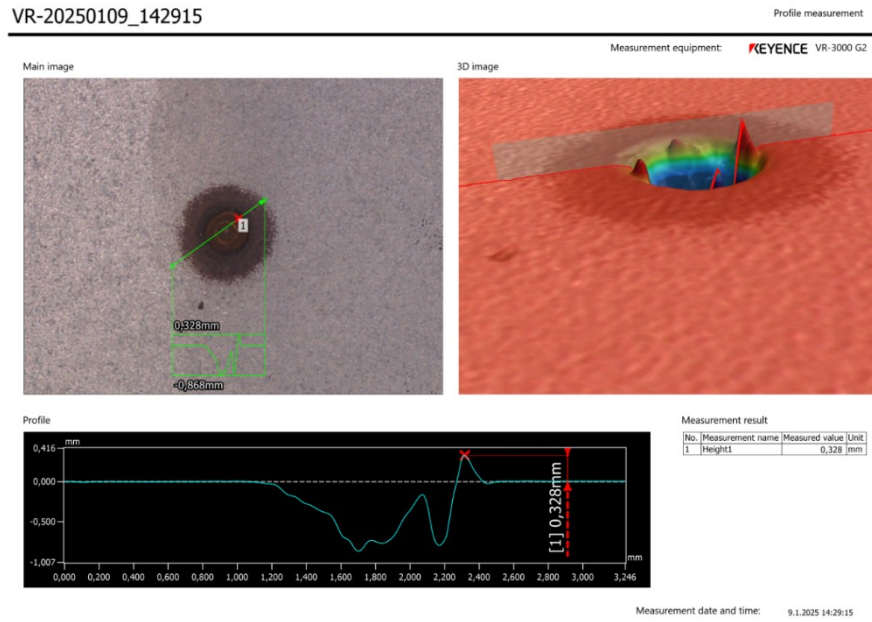


Figure 26. Highest measured spot welds protrusion

The highest laser power was applied in the experiments with 900 W core power, 600 W ring power and 150 ms interaction time (parameter 8), resulted in a 243 μm protrusion which is depicted in Figure 27.

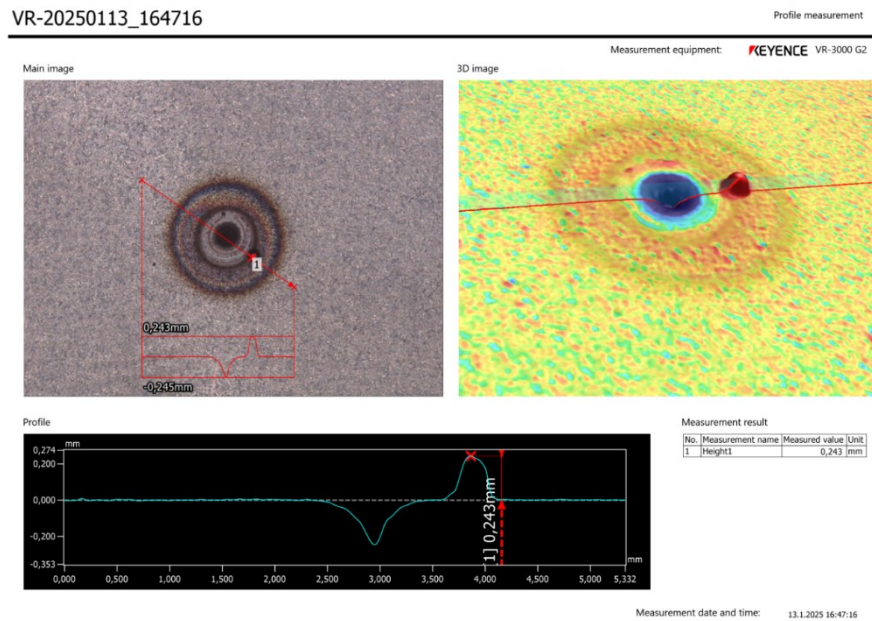


Figure 27. Weld height for parameter 8 (900 W,600 W, 150 ms)

The spot protrusion measurement results (Table 5), show that at least one spot in each parameter exhibits a significantly higher value compared to other spots. The average value of spot protrusion for each set of test specimens involving twelve values (both sides) was also calculated and presented in Table 5. A comparison of the results is shown in Figure 28. The outcomes indicate that the minimum protrusion average (48 μm) which could be considered as the optimal result, was achieved in the maximum applied ring power with extended interaction time. The graphs in Figure 28 also exhibit that the average protrusion in 100 millisecond interaction time remains relatively consistent across various ring power levels, whereas these values at 150 ms illustrate more pronounced variations between data points.

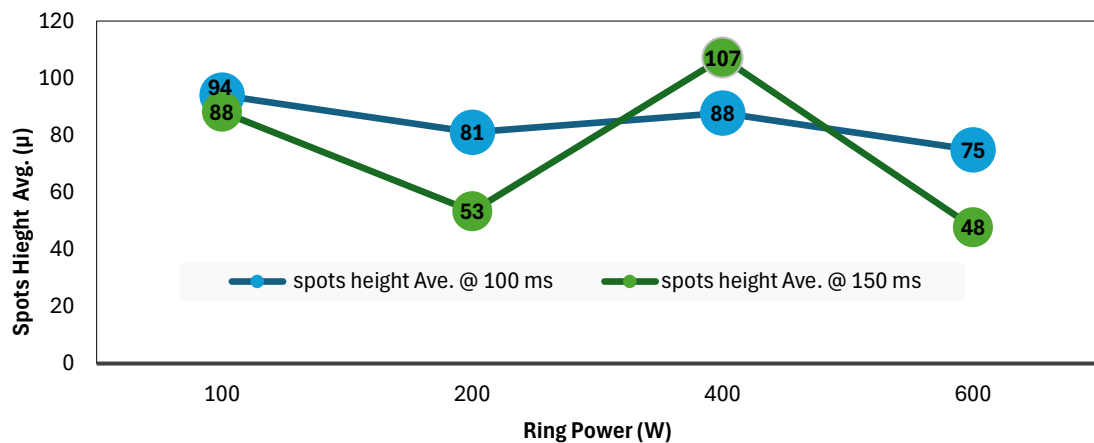


Figure 28. Spots average height versus Ring Power at 100 & 150 ms interaction time

Observation of the spot surface in all scanned 3D images reveals a smooth surface, and weld spots protrusion appears to be primarily influenced by negative effects of molten material ejection. In conclusion, the weld protrusion is relatively more stabilized with lower beam interaction times and overall reduces with increasing ring power. Further analysis is needed to determine the weld protrusion is a spatter or a weld reinforcement along the periphery of the weld. Nevertheless, post-processing is required in both cases and the process needs to be optimized in a way that it reduces the occurrences of heavy spatter and the formation of a very large weld reinforcement. Spatters can be primarily controlled by optimizing the cooling rates leading to a much more stabilized melt pool whereas weld reinforcement could

be controlled by depth of penetration. With a higher depth of penetration, there is a less possibility of the material flowing upwards and solidifying as a reinforcement.

5.2 Tensile-Shear Test

In the next step, as previously mentioned, the tensile-shear test was conducted and, in this section, the tested samples are analysed to evaluate their mechanical behavior. The laser spot welds are applied perpendicular to the surface of samples; therefore, the Tensile-Shear test evaluation is considered in the following steps. The thin sheets were subjected more to the tensile load, whereas the LSWs were more prone to shear. The force-displacement response for each of the specimens based on table 3 is assessed.

Figure 29 demonstrates the force-strain curves for the lowest ring power for both interaction times 100 ms and 150 ms. As stated in the experimental section for each set of parameters, three replicas were tested, hence the graphs compare the behavior of these samples.

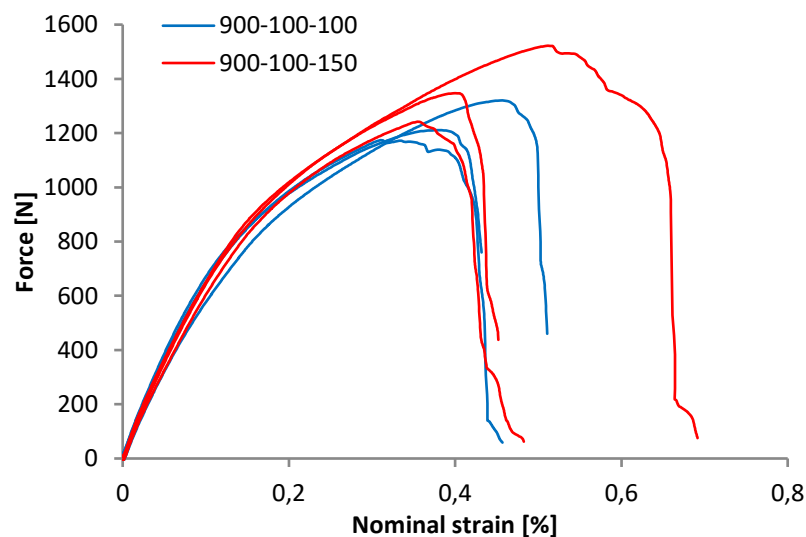


Figure 29. Force-Strain curve for 1st and 2nd set of parameters

The recorded test results for three samples as indicated in blue solid lines for 100ms indicate a maximum average force of 1235 N. This value increased to 1370 N as the interaction time was extended from 100 to 150 ms. The Force-Strain curves behaviour of the samples

approves that the second parameters with increased interaction time tend to reach higher levels of maximum force values and almost similar strain levels compared to the first sets, suggesting improved strength and greater withstanding against load and deformation.

In the next experimental set, the ring power was doubled to 200 W in the consistent core power of 900 W, while the time again increased from 100 to 150 ms and the result is shown in Figure 30.

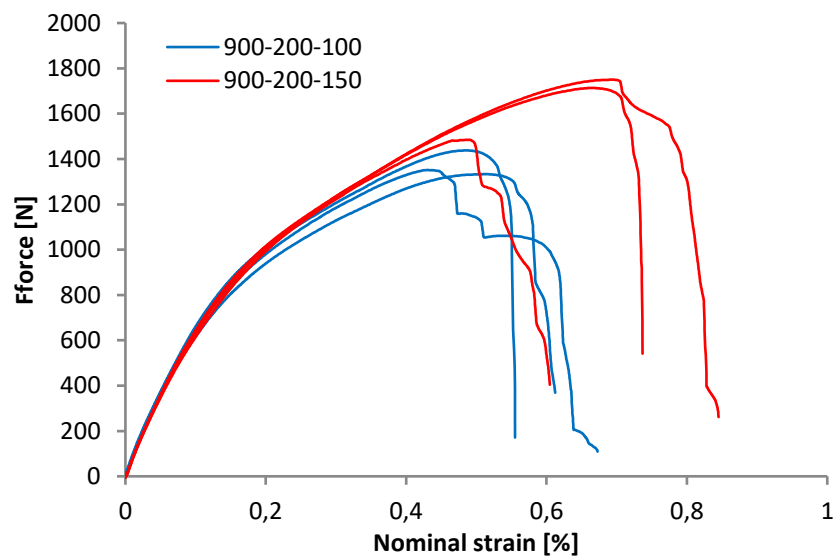


Figure 30. Force-Strain curve for 3rd and 4th set of parameters

Similar behavior was achieved while interaction time increased. Samples with lower interaction time reached lower peak force values, and weld spots failed at lower strain levels. The maximum average force at 100 ms interaction time was 1374 N, increasing to 1649 N at 150 ms. In the subsequent test samples, the ring power was doubled again to 400 W and the outcomes are illustrated in Figure 31.

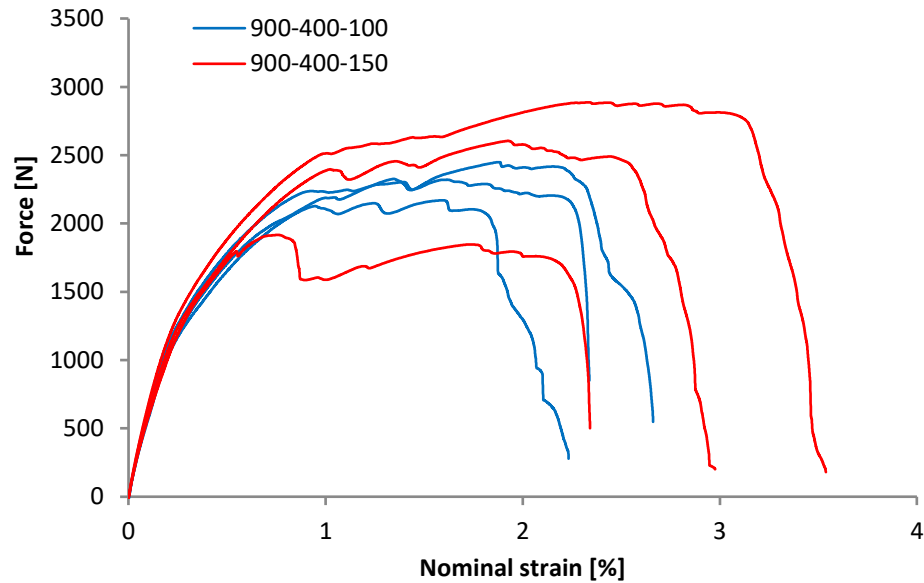


Figure 31. Force-Strain curve for 5th and 6th set of parameters

The results, similar to the two previous sets of experiments, indicate that increasing the ring power and interaction time exhibits higher maximum breaking force and greater strain at failure value, however, the increase is more significant in this case. The graphs for both sets of samples also represent that the gradual decline after the peak force and sustaining load for a longer period before failure, suggest higher overall strength, improved energy absorption and greater resistance to sudden failure. The highest average force at 100 ms was 2314 N representing an increase to 2470 N at 150 ms. Comparing these force values with the previous set of parameters demonstrates approximately a 70 % increase at 100 and a 50 % increase at 150 ms.

The final experimental arrangements involved the highest laser power which was performed in the design of this study and is depicted in Figure 32. The ring laser power in these sets of parameters was increased to 600 W.

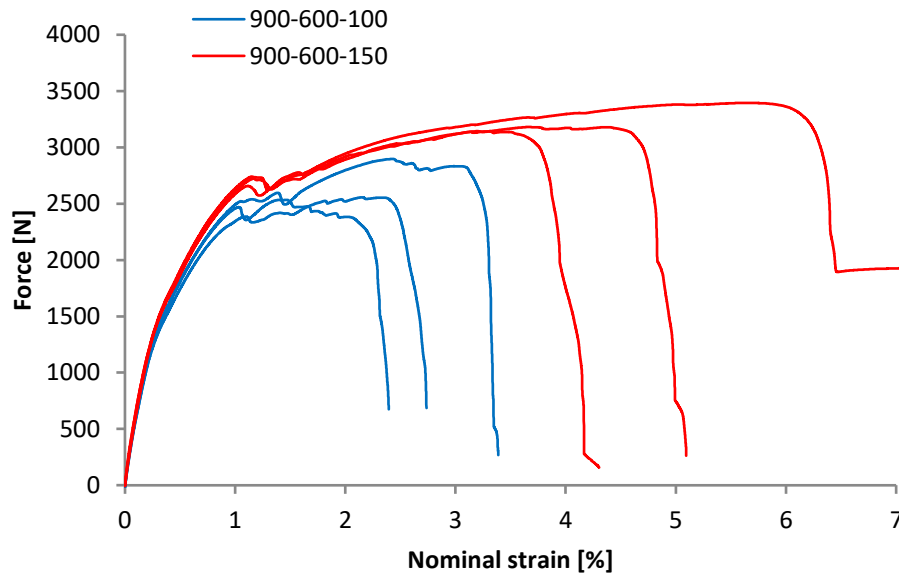


Figure 32. Force-Strain curve for 7th and 8th set of parameters

The analysis of the last Tensile-shear test graphs presents that results follow relatively the same pattern as previous observations but with an even more pronounced increase in maximum force and displacement. The maximum average load increased from 2663 N to 3240 N while interaction time extended from 100 to 150 ms, showing a notable increase compared to the previous set of parameters. This set of parameters demonstrates considerably higher strain at failure for both 100 and 150 ms of interaction times. The fluctuation after the peak load in the 8th parameter (900-600-150) is less than the previous parameters with 400 ring power, suggesting a more stable failure mechanism. In all previous set of experiments and corresponding graphs, the failure occurred in the weld spots. However, one of the three specimens in the last parameter (600 W ring power at 150 ms), failure occurred in the SS thin-sheet, as shown in Figure 33.

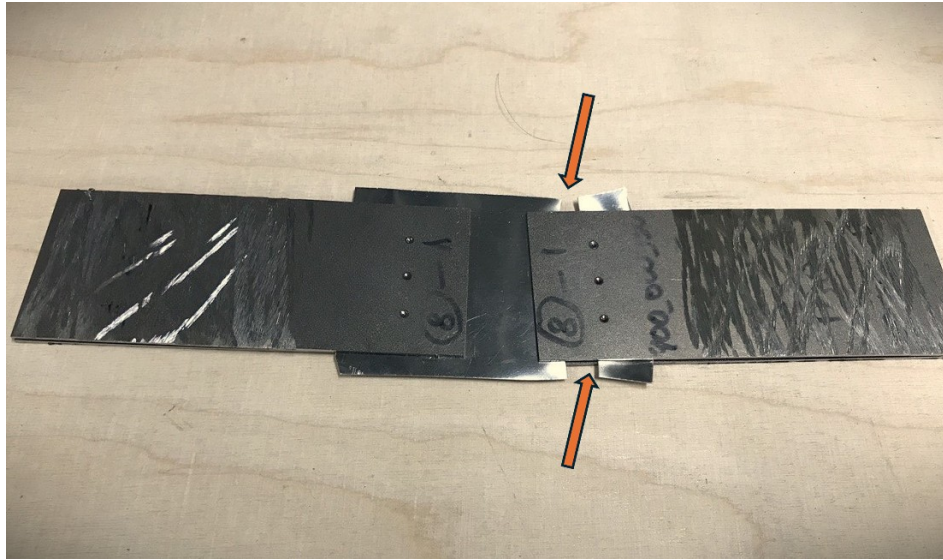


Figure 33. Failure in SS thin sheet

The fracture appearance of laser spot welded joints also showed that at lower laser power (100 and 200 W ring power), the fracture was interfacial (Figure 34 a). However, at the higher sets of laser power (400 and 600 W ring power), the samples began to partially pull out and then fracture continued to tear by the stainless steel base material as demonstrated in Figure 34 b. This could be a critical result as greater laser power and longer interaction time may keep the spot joints beyond the strength of SS sheets.

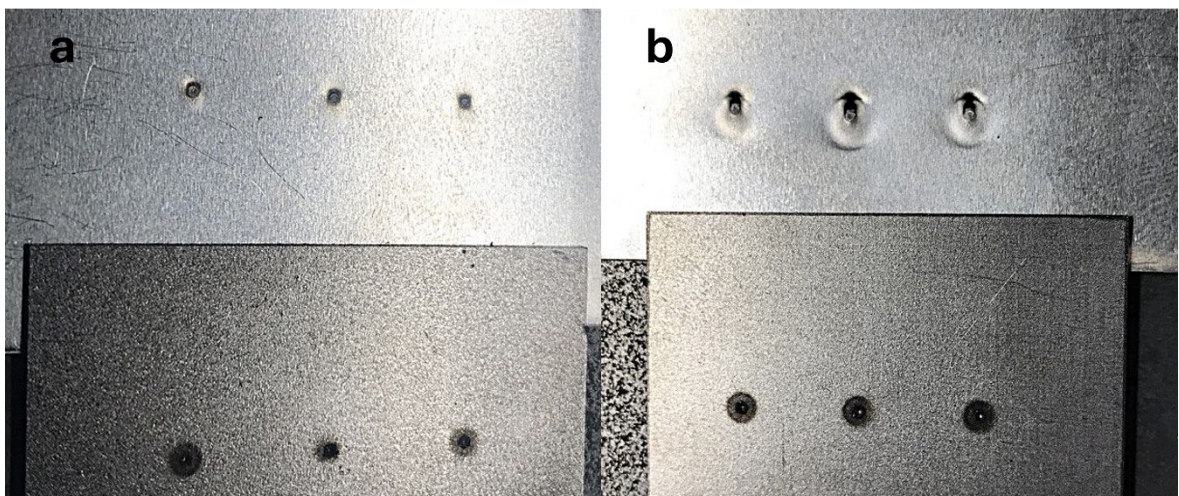


Figure 34. (a) Interfacial fracture in sample 4 (900W-200W-150 ms) (b) partially Pulled out and tearing in SS in Sample 6 (900W-400W-150ms)

Tensile test results also provided information about the displacement of joints and the peak of force sustained by specimens for various ring power and interaction times. Table 5 represents the average maximum force and displacement for all parameters.

Table 5. F_{\max} Avg. and dL in F_{\max} Avg.

Parameter Set	dL at F_{\max} Avg. (mm)	F_{\max} Avg. (N)
1	0,19	1235
2	0,22	1370
3	0,27	1374
4	0,35	1649
5	1,23	2314
6	1,20	2470
7	1,48	2663
8	3,40	3240

Figure 35 shows that displacement at average Fmax relatively increases when laser power and interaction time increase across different parameters.

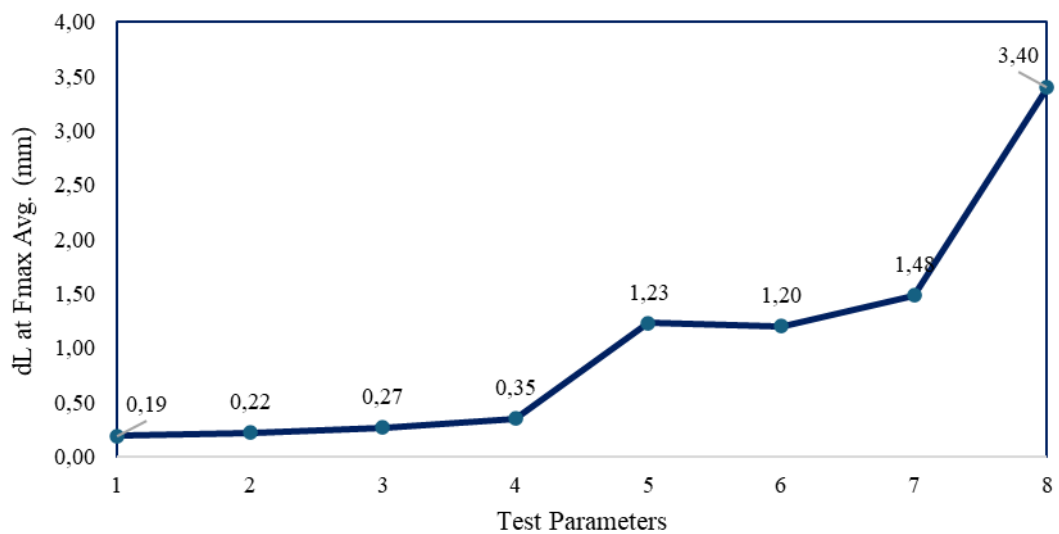


Figure 35. Displacement in Average Maximum Force

Figure 36 compares changes in average F_{\max} across different ring power and interaction times.

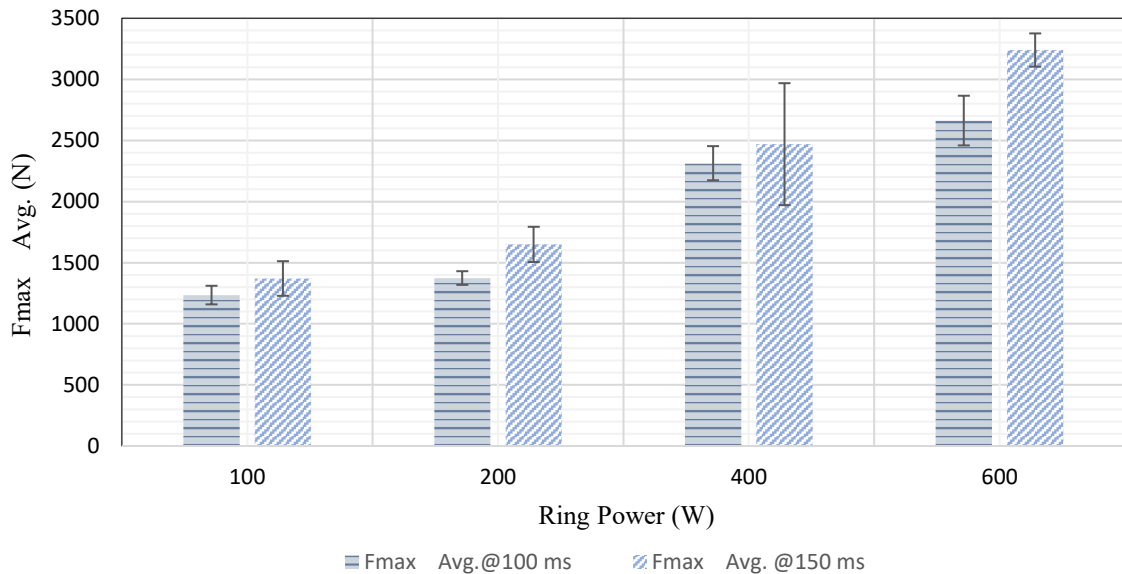


Figure 36. Deviation in Fmax at different set of parameters

This chart confirms that, in each set of parameters, samples with a 150-millisecond interaction time, tend to exhibit higher average force values. It also represents that increasing the interaction time from 100 to 150 ms at lower laser power has a relatively smaller effect compared to 400 and 600 W ring power. At the higher laser power, increasing in force values becomes more significant.

The following analysis compares the maximum average force values and maximum laser spot weld protrusion across different laser ring power levels and interaction times. Figures 36 and 37 demonstrate these comparisons. As stated in the experimental section, the highest protrusion in each set of parameters was identified. Therefore, maximum weld protrusion height, represents the highest value among the six LSW on both sides at each set of parameters. Figure 37 displays changes in F_{\max} and LWS protrusion at 100 ms interaction time as ring power increases.

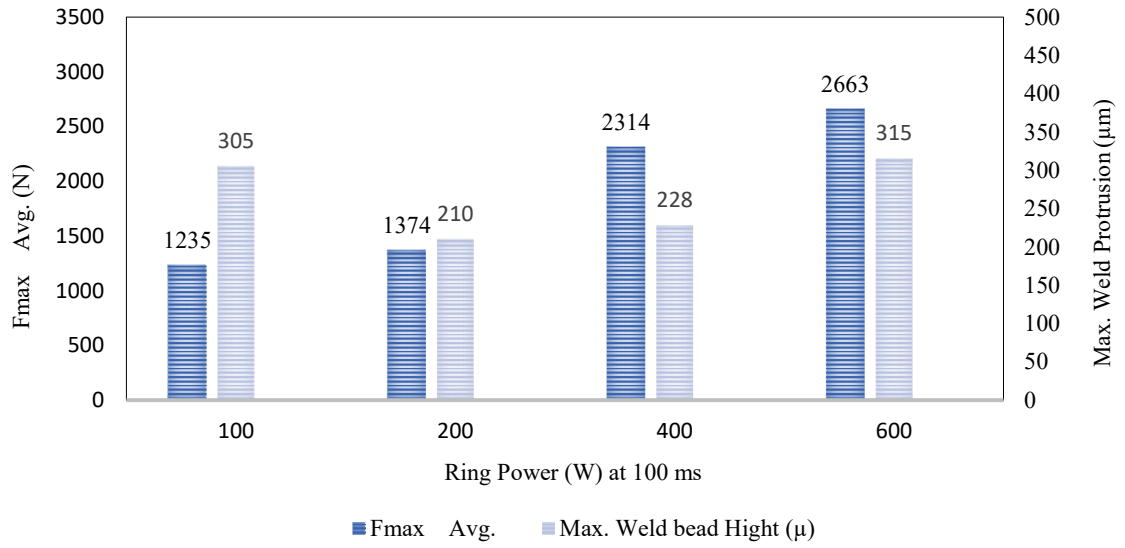


Figure 37. F_{max} Avg. & Max. LSW protrusion in different Ring powers at 100 ms

Changes in F_{max} and laser spot welds protrusion are observed as ring power increases at an interaction time of 150 milliseconds, as demonstrated in Figure 38.

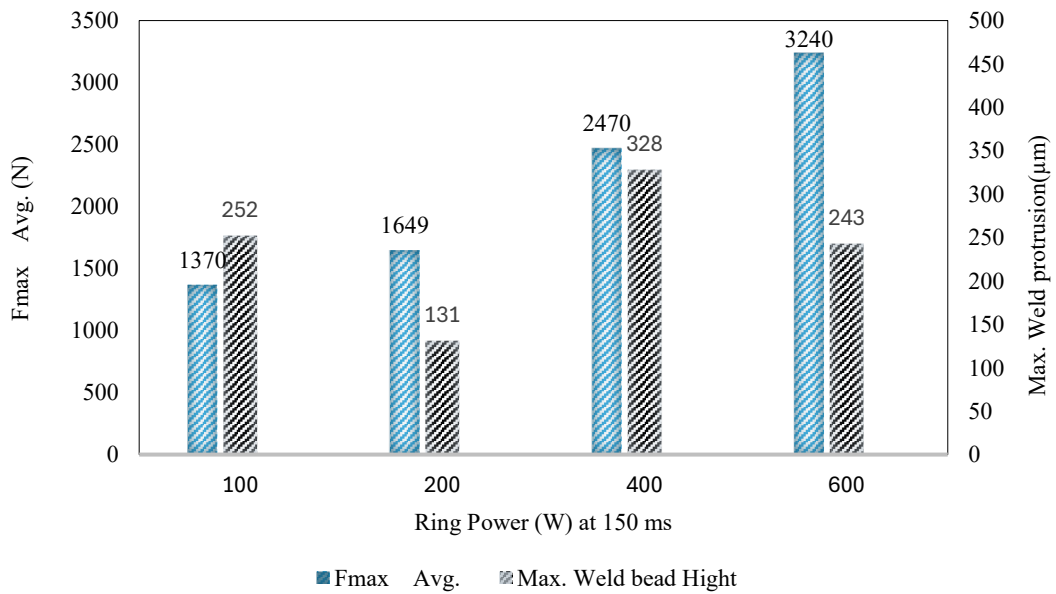


Figure 38. F_{max} Avg. & Max. LSW Height in different Ring powers at 150 ms

Comparing these graphs indicates that, while increasing laser power, promotes the maximum force values at both 100 and 150 interaction time, exhibiting stronger welded joints, the spot protrusion value varies and shows fluctuation. The most promising result appears to have been achieved at the highest ring power (600 W), where increasing interaction time from 100 to 150 led to a rise in the maximum force and a reduction in the highest weld spot protrusion from 315 to 243 μm . The result was further supported by the data from Table 4. But it is important to note that at higher interaction times of 150ms process seems to be more unstable indicated by higher variability in the Force strain curves. With higher interaction time, a higher amount of material is melted and therefore susceptible to more weld defects. This opens up further scope of research regarding controlling the deviation in higher interaction time but still achieving the highest mechanical strength and lowest overall weld protrusion.

5.3 Cross Section of Weld Spots

The weld morphology of laser spot welds, significantly affect the mechanical properties and performance of laser spot welded joints. Since the laser welding technique is applied from one side, the fusion area represents asymmetric shape and dimensions. Moreover, differences in thermal conductivity and heat absorption of dissimilar metals affect the formation and growth of spot welds (Torkamany, Sabbaghzadeh & Hamedi, 2012, p. 667). Since in the tensile-shear test, the force was applied to the interface between the upper and lower surface of the SS layer in conjunction with MS sheets, particularly in the weld spot area, evaluating the cross-section of the weld spot plays a significant role in understanding joint performance. Therefore, the cross-section of all sets of parameters was prepared and images were captured using an optical microscope as shown in Table 6. and interface width between SS and MS was measured utilizing a laser profilometer. Figure 39 illustrates a microscopic image and the width measurement of one sample as an example.

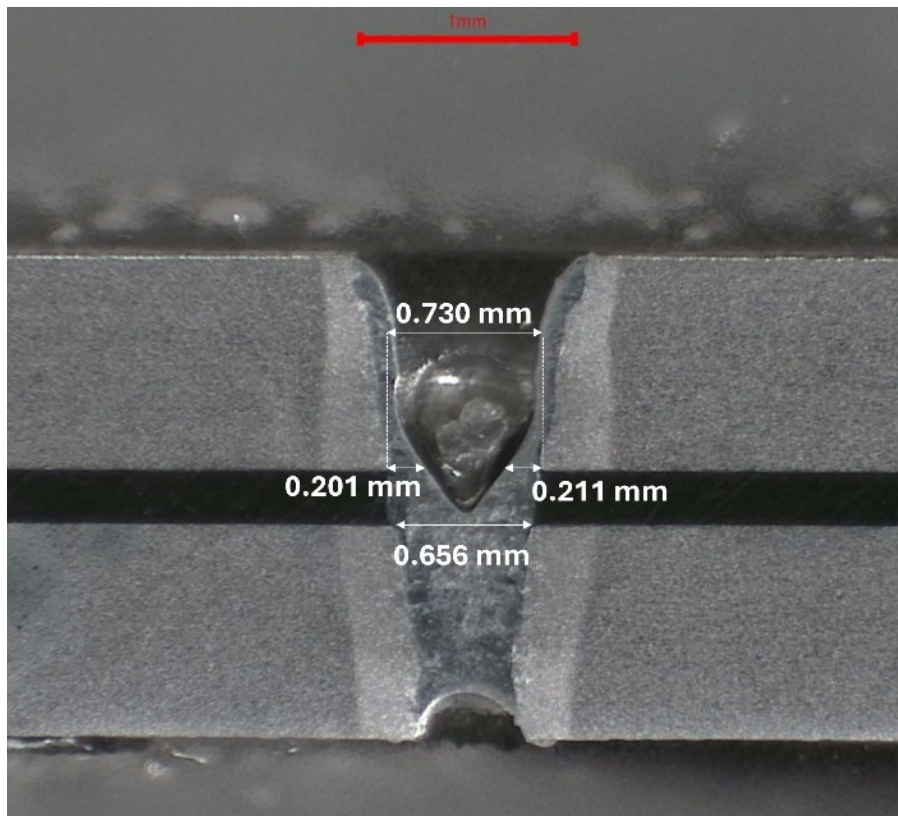


Figure 39. Microscopic image and interface measurement of SS and MS in parameter No 4 (900-200-100)

Table 6, demonstrate cross-section of laser spot weld for all set of parameters.

Table 6. Cross-Section images of LSWs

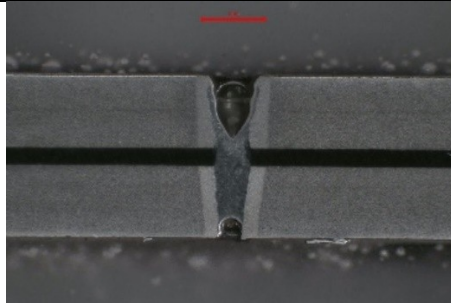
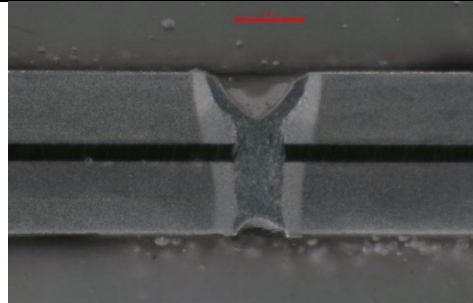
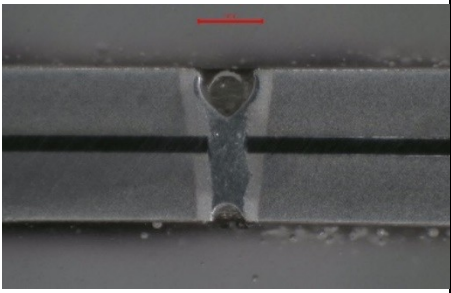
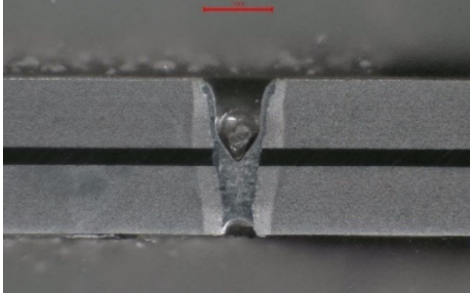
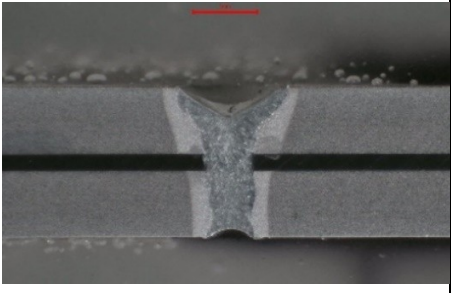
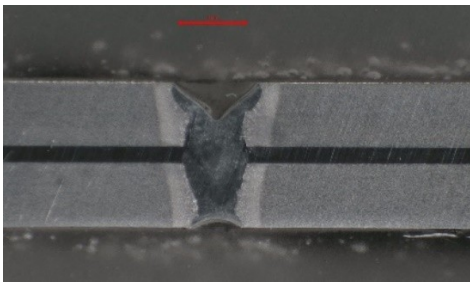
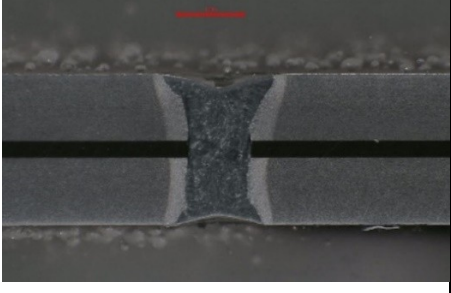

Core Power (W)	Ring Power (W)	Interaction Time (ms)	
		100	150
900	100		

Table 7 continues. Cross-Section images of LSWs

Core Power (W)	Ring Power (W)	Interaction Time (ms)	
		100	150
900	200		
	400		
	600		

The schematic of the interfaces between MS and SS is depicted in Figure 40 and all interface width measurements are displayed in Table 7.

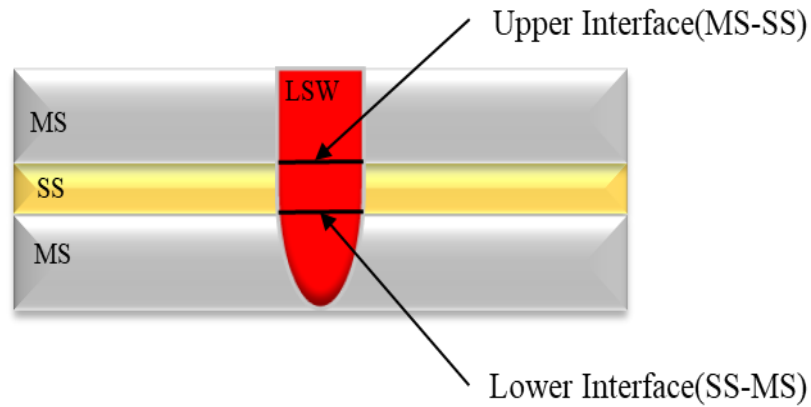


Figure 40. Schematic of upper and Lower interface in a LSW

Table 8. Widths of Upper and Lower interface area between MS & SS

Sample	Upper Sheet interface width (mm)	Lower Sheet interface Width(mm)	Avg. Width Value (mm)
1	0,574	0,535	0,555
2	0,774	0,790	0,782
3	0,604	0,653	0,629
4	0,730 (0,201–0,211)	0,656	0,693
5	0,811	0,763	0,787
6	0,890	0,941	0,916
7	0,967	1,015	0,991
8	1,230	1,160	1,195

The measurement of all spots cross-sections in the interface region and relevant calculated interface area between SS and MS is given in Table 8.

Table 9. Values of Upper and Lower interface area between MS & SS

Sample	Upper interface Area (mm ²)	Lower interface Area (mm ²)	Avg. Area Value (mm ²)
	MS-SS	SS-MS	
1	0,26	0,22	0,24
2	0,47	0,49	0,48
3	0,29	0,33	0,31
4	0,34	0,34	0,34
5	0,52	0,46	0,49
6	0,62	0,70	0,66
7	0,73	0,81	0,77
8	1,19	1,06	1,13

Figure 41 compares how these areas behave across all sets of test samples.

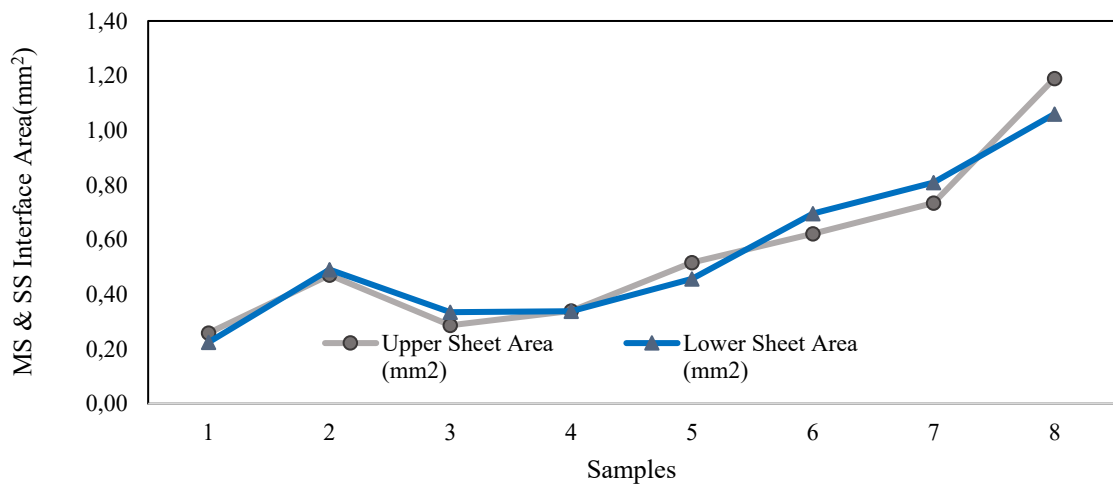


Figure 41. Comparing Upper and Lower interface area

The interface area between the laser spot welded thin sheet metallic parts was subjected to shear stress. The measurements and graphs in Table 8 and Figure 40 represent a general upward trend in both upper and lower areas at 100 and 150 ms. The results do not indicate a stable behaviour in determining whether the upper or lower joint surface has a greater

interface area in each set of parameters. However, the maximum shear surface was obtained in the upper interface area, when the highest ring power (600 W) was applied at 150 ms.

5.4 Statistical Analysis for Taguchi design

In section 4.2.1 of this thesis, it detailed how the Taguchi design of experiments was utilized, and subsequent experimental tests were conducted accordingly. In this section, the statistical analysis is briefly discussed based on the obtained results. The results which are considered as results are: (a) maximum force in tensile-shear test, (b) average of weld bead spot protrusion and (c) average of interfaces area between MS and SS. In the Taguchi design, there are some control factors, that are procedure parameters which can be controlled. Noise factors are those which cannot be controlled during the procedure but can be controlled in experimentation. The higher signal-to-noise(S/N) indicates control factor settings that decrease the effects of the noise factors and are desired. Table 9 displays the design of the experiment, its results and their relevant Signal-to-Noise ratio for all set of parameters

Table 10. Signal to Noise ratio for set of parameters

Core Power(W)	Ring Power (W)	Interaction Time(ms)	Fmax (N)	S/N Ratio (Fmax)	Avg Weld Spots Protrusion(μ)	S/N Ration (Protrision)	Avg. Interface Area (mm ²)	S/N Ratio (Area)
900	100	100	1235	61,83	94	-39,46	0,24	-12,40
900	100	150	1370	62,74	88	-38,89	0,48	-6,38
900	200	100	1374	62,76	81	-38,17	0,31	-10,17
900	200	150	1649	64,35	53	-34,49	0,34	-9,37
900	400	100	2314	67,29	88	-38,89	0,49	-6,20
900	400	150	2470	67,85	107	-40,59	0,66	-3,61
900	600	100	2663	68,51	75	-37,50	0,77	-2,27
900	600	150	3240	70,21	48	-33,62	1,13	1,06

Figure 42, illustrate the main effect plots for mean of maximum force S/N ratio across all set of parameters.

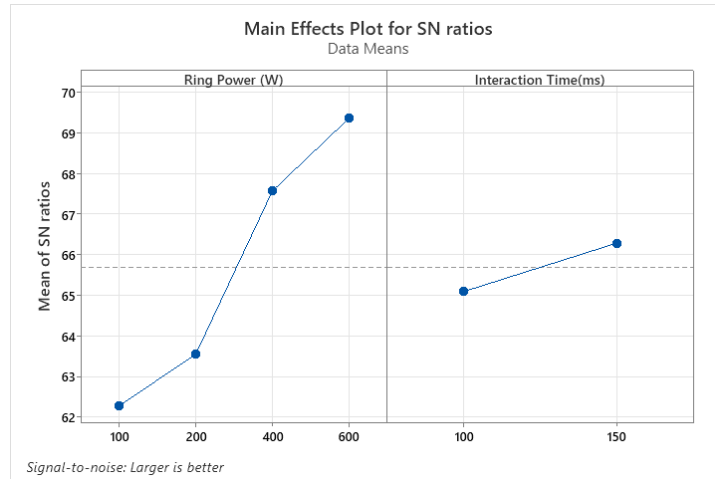


Figure 42. Main effects plots for SN ratios - maximum forces

The Taguchi analysis indicates that ring power in level 4 (600 W) and interaction time in level 2 (150 ms) presented higher signal-to-noise ratios, indicating that laser power plays a more significant role in the experimental evaluation of maximum force.

For laser spot welds, minimum protrusions are desired in this study. The Taguchi analysis indicated that the highest SN ratios, which indicate the lowest LSW protrusion, were attained at the fourth level of ring power and the second level of interaction time in the average protrusion of spots across all sets of parameters. In this case, the laser power also ranked higher and had a greater impact on the experimental evaluation. Figure 43 illustrates fluctuations in the mean of SN ratio for ring power.

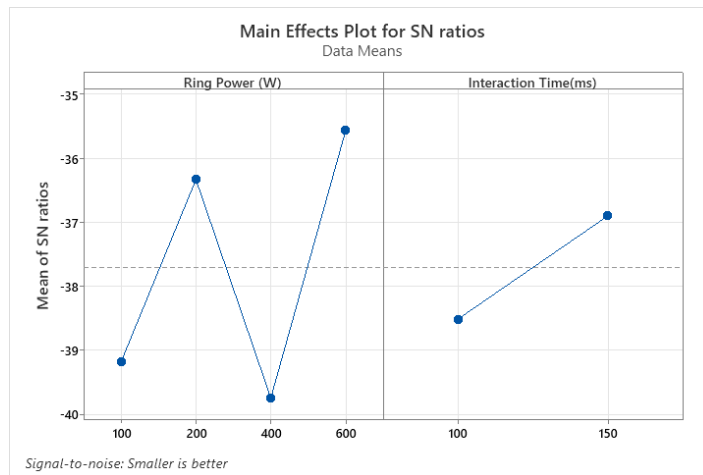


Figure 43. Main effects plots for SN ratios - Average LSW protrusion

The final Taguchi analysis results represent the mean value of SN ratios for the joints average interface area. This analysis again shows that 600 W ring power and 150 milliseconds interaction time indicates the highest S/N ratios and laser power had stronger effects on the analysis (Figure 44).

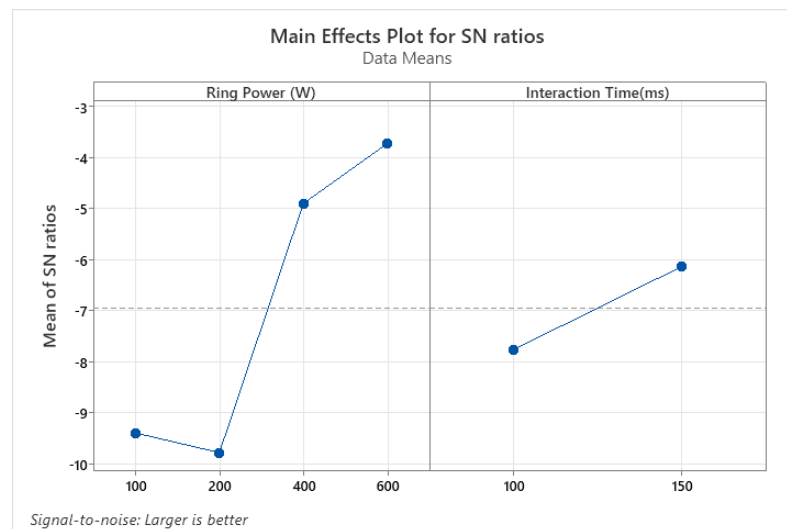


Figure 44. Main effects plots for SN ratios- Average Interface Area

The results of Taguchi statistical analysis obtained from Minitab software indicated that, at a constant laser core power, ring power had a more significant influence in this analysis

compared to interaction time, and at level 4 of the DOE with 600-W ring power, the most desirable results were gained. The Taguchi design also enables applications of analysis of variance (ANOVA) for parameters to assess the results. The P-value determines whether a parameter is statistically significant or just due to random chance. If the P-value is < 0.05 , it represents that the difference between values is statistically significant and the null hypothesis can be rejected, meaning a parameter has an effect, otherwise (P-value > 0.05), shows the tested parameters might not have a strong effect. (Raftar, Ahola, Lipiäinen & Björk, 2023, pp. 8–9.) The results showed that ring power provided the most statistically significant influence on maximum sustained force in laser spot welded joints, as evidenced by P-value < 0.05 obtained from the one-way ANOVA analysis in Minitab.

5.5 Summary

The evaluation of laser spot protrusions in welded thin sheets revealed a pronounced variation and occasional fluctuation in weld protrusion height across all spots. The measurements by profilometer indicated that, regardless of consistency in parameters, some spots exhibited excessive protrusion height while most maintained relatively low protrusion. The observed scattered protrusion on both sides appeared to result from material ejection, indicating dynamic instability and metallurgical inconsistencies during laser interaction. The stacking nature of thin sheet assembly in the EV rotors emphasizes the importance of minimizing the protrusion fluctuations of spots that could lead to increased inter-layer gaps, misalignments, reduced mechanical properties, and increased post-processing works, making it a critical factor requiring more investigation.

The recorded results from the tensile-shear test and the maximum force-displacement curves for all sets of parameters were demonstrated and evaluated. This analysis aimed to assess the influence of laser power and interaction time on mechanical strength, deformation behaviour and failure mode of laser spot welded MS-SS thin sheet stacks. In each set of parameters, maximum force and strain value increased as interaction time is increased from 100 ms to 150 ms. Similar trend is observed when ring power is increased. Therefore, the results indicated improvement in maximum force and laser spots strength.

Additionally, the F_{\max} -strain curves at lower laser ring power (100 and 200 W) demonstrated short tails after failure with relatively sudden drops after the peak load. In these cases, the

laser spot welded joints showed interfacial fracture. However, at the higher laser ring power levels (400 W and 600 W), the curves represented longer tails after the peak load, and the fracture was partially pulled out, and continued with tearing. Fluctuations after the maximum force in 600 W ring powers were less pronounced compared to those at 400 W power, while the extent of tearing was greater. The results also suggested that increasing the laser power may cause failure in SS base material. In the last and highest level of power and interaction time, one sample failed from the SS thin layer, indicating higher strength in the spot-welded joints. Furthermore, the results indicated that failure mechanisms at lower laser power were mostly shear whereas at higher power were more likely tensile. The transition was observed at approximately 2100 N, based on the recorded result of the tensile test machine. The progressive increase in displacement measurement at peak loads, suggests improved ductility and energy absorption capacity at higher laser power and longer interaction time. However, the highest displacement (3,4 mm) led to failure in base material in one sample at 600 W and 150 ms, potentially indicating structural risks and misalignments in real applications of laser spot welded thin sheets such as rotors stacks.

The cross-section evaluation of laser spot welded thin layers of MS and SS was also challenging. The width measurement and area calculation of all spots represented general upward behaviour with higher laser power and prolonged interaction time. The cross-section evaluation of LSW samples demonstrated narrower HAZ and more integrity in 100 ms time. Observation showed imperfections in samples at both 100 and 150 ms and these imperfections were more obvious at higher interaction times. Since stainless steel has lower thermal conductivity than the mild steel, it was expected that the lower interfacial area would be smaller. However, deviations were observed in some cases. These unexpected results require more evaluation and investigation. It is worth mentioning that the spots size and diameter were very small, making it particularly challenging to achieve the exact centered cross-section of each spot during fine grinding and polishing, which may have affected the accuracy of the results.

6 Conclusion

This thesis conducted a comprehensive analysis of laser spot welding as a novel method of joining thin sheet dissimilar material, Stainless Steel 316L and Mild Steel 340LA, for Synchronous Reluctance Motors and high-speed electrical appliances. The aims categorised to measure laser spots protrusion height, mechanical properties analysis and cross-section evaluation of laser spot welded joints. The Taguchi method utilized for design of experiments and laser core power, ring power and interaction time were considered as main parameters. The spots protrusion measurements illustrated a randomized height pattern for all set of parameters regardless of laser power and time changing. The tensile-shear test, however, indicated that higher laser power and prolonged interaction time significantly effect on maximum sustained force and strain behaviour of laser spot welded joints. The result showed that the maximum average force increased from 1235 N to 3240 N, and average displacement at maximum average force increased from 0.19 mm to 3.40 mm, presenting pronounced improvement. Additionally, the failure mode transitioned from shear at lower laser power to tensile at higher laser power. The cross-sectional evaluation represented narrower HAZ and relatively more integrated welds at lower interaction time, while the average upper and lower interfacial area between thin sheets generally increased from 0.24 mm² at lowest laser power to 1.15 mm² at highest laser power, emphasizing higher weld strength at higher laser power.

6.1 Further Research

This thesis provided a functional yet comprehensive characterization for laser spot welding of thin sheets. Further studies could be conducted to assess the microstructural and metallurgical reasons behind the randomized pattern in the spot's protrusion. This would be helpful to achieve a smoother surface, reducing excessive post-processing work in real applications. Additionally, this study concentrated on laser spots welding, therefore more research can explore alternative techniques of laser welding such as linear, spiral or concentric circle welding to evaluate their behavior on dissimilar thin sheet materials. This

would help obtain more possible optimized parameters with even less interaction time and decrease the manufacturing process time in future mass production scenarios.

References

- Abramenko, V., Nerg, J., Petrov, I., & Pyrhönen, J. (2020). Influence of magnetic and nonmagnetic layers in an axially laminated anisotropic rotor of a high-speed synchronous reluctance motor including manufacturing aspects. *IEEE Access*, 8, Pp .117377–117389.
- Ai Y, Jiang P, Wang C, Mi G and Geng S (2018) Experimental and numerical analysis of molten pool and keyhole profile during high-power deep-penetration laser welding. *International Journal of Heat and Mass Transfer* 126:1, Pp. 779–789.
- Allahyari A, Petrov I, Pyrhönen J, Aarniovuori L, Lindh P and Parviainen M (2024) Design and Optimization of a Bridgeless Rotor for Synchronous Reluctance Machines. *IEEE Access*, 12. Pp. 65825-65837.
- Bonthu, S. S. R., Arafat, A., & Choi, S. (2017). Comparisons of rare-earth and rare-earth-free external rotor permanent magnet assisted synchronous reluctance motors. *IEEE Transactions on Industrial Electronics*, 64(12), Pp. 9729–9738.
- Bremer, S. J. L., Aarts, R. G. K. M., & Römer, G. R. B. E. (2024). Design and implementation of dynamic beam shaping in high power laser processing by means of a Deformable Mirror. *Optics and Laser Technology*, 177: 111066. Pp. 1-12.
- Chai, X., & Dong, Y. (2024). Rotor design and optimization of synchronous reluctance machine with low torque ripple. *Journal of Power Electronics*, 25, Pp-360-369.
- Credo, A., Petrov, I., Pyrhönen, J., & Villani, M. (2022). Impact of manufacturing stresses on multiple-rib synchronous reluctance motor performance. *IEEE Transactions on Industry Applications*, 59(2), Pp. 1253–1262.
- Dziechciarz, A., Oprea, C., & Martis, C. (2016). Multi-physics design of synchronous reluctance machine for high-speed applications. 42nd Annual Conference of the IEEE Industrial Electronics Society, Florence, Italy, 2016. Pp.1704–1709.
- Gerlach ME, Zajonc M and Ponick B (2021) Mechanical stress and deformation in the rotors of a high-speed PMSM and IM, *Mechanischer Stress und Verformung in den Rotoren einer Hochdrehzahl-PMSM und einer Hochdrehzahl-IM*. *Elektrotechnik Und Informationstechnik* 138 (2021), Nr.2 138(2), Pp. 96–109.

Heidari, H., Rassölkin, A., Kallaste, A., Vaimann, T., Andriushchenko, E., Belahcen, A., & Lukichev, D. V. (2021). A review of synchronous reluctance motor-drive advancements. *Sustainability*, 13(2), Pp. 1-37.

Katayama, S. (2020). *Fundamentals and details of laser welding* (1st ed.). Springer Singapore, 198p.

Kim, H., Park, Y., Oh, S., Jang, H., Won, S., Chun, Y., & Lee, J. (2020). A study on the rotor design of line start synchronous reluctance motor for IE4 efficiency and improving power factor. *Energies*, 13(21), Pp. 1-15.

Kuryntsev, S. (2021). A review: laser welding of dissimilar materials (Al/Fe, Al/Ti, Al/Cu)—methods and techniques, microstructure and properties. *Materials*, 15(1), Pp. 1-30.

Leuning, N., Steentjes, S., Hameyer, K., Gerhards, B., & Reisgen, U. (2017). Analysis of a novel laser welding strategy for electrical steel laminations. *7th International Electric Drives Production Conference (EDPC)*. Würzburg, Germany, 2017, Pp 1–8.

Li, Q., Mu, Z., Luo, M., Huang, A., & Pang, S. (2021). Laser spot micro-welding of ultra-thin steel sheet. *Micromachines*, 12(3), Pp. 1-12.

Martinson, P., Daneshpour, S., Koçak, M., Riekehr, S., & Staron, P. (2009). Residual stress analysis of laser spot welding of steel sheets. *Materials in Engineering*, 30(9), Pp. 3351–3359.

Raftar, H. R., Ahola, A., Lipiäinen, K., & Björk, T. (2023). Simulation and experiment on residual stress and deflection of cruciform welded joints. *Journal of Constructional Steel Research*, 208, Pp. 1-12.

Seibold, M., Schrickler, K., Schmidt, L., Diegel, D., Friedmann, H., Hellwig, P., Fröhlich, F., Nagel, F., Kallage, P., Rack, A., Requardt, H., Chen, Y., & Bergmann, J. P. (2024). Temporal and spatial determination of solidification rate during pulsed laser beam welding of hot-crack susceptible aluminum alloys by means of high-speed synchrotron X-ray imaging. *Journal of Advanced Joining Processes*, 10, Pp. 1-11.

Shealy, D. L. (2000). Theory of geometrical methods for design of laser beam shaping systems. Paper presented at the Laser Beam Shaping, 4095. Pp. 1–15.

Singh, S., Petrov, I., Sergeant, P., & Pyrhonen, J. (2024). Optimisation of Slot Wedges for 27 kW 100 krpm Axially Laminated Synchronous Reluctance Machine. *IEEE International Conference on Industrial Technology (Online)*. IEEE, 2024, Pp. 1–6.

Taghavi, S., & Pillay, P. (2014). A sizing methodology of the synchronous reluctance motor for traction applications. *IEEE Journal of Emerging and Selected Topics in Power Electronics*, 2(2), Pp. 329–340.

Tang, Z., Zhang, X., Wan, L., Ouyang, Y., Gao, Z., Wei, Q., Wang, A., Yang, H., Wu, Y., & Zhang, Y. (2023). Blue laser welding of laminated electrical steels: Dynamic process, weld bead characteristics, mechanical and magnetic properties. *Journal of Materials Processing Technology*, 312, Pp. 1-9.

Torkamany, M. J., Sabbaghzadeh, J., & Hamedi, M. J. (2012). Effect of laser welding mode on the microstructure and mechanical performance of dissimilar laser spot welds between low carbon and austenitic stainless steels. *Materials & Design*, 34, Pp. 666–672.

Wang, Z., Jiang, M., Chen, X., Du, Y., Lei, Z., Zhao, S., & Chen, Y. (2024). Mitigating spatters in keyhole-mode laser welding by superimposing additional ring-shaped beam. *Optics and Laser Technology*, 168, Pp. 1-13.

Zhang, X., Tang, Z., Di, S., Wang, H., Wu, Y., & Wang, H. (2024). Effect of defocus on blue laser spot welding of electrical-steel-laminations. *Optics & Laser Technology*, 175, Pp. 1-11.

Ziegler, M., Brandl, F., Kuehl, A., & Franke, J. (2021). Evaluation of Laser-welded Electrical Steel Laminations for Electric Motors. *12th International Symposium on Advanced Topics in Electrical Engineering (ATEE)*, Friedrich-Alexander-Universität Erlangen-Nurnberg (FAU), Nuremberg, Germany, 2021, Pp, 1–6.

Ziegler, M., Mayr, A., Seefried, J., Kuehl, A., & Franke, J. (2019). Potentials of process monitoring during laser welding of electrical steel laminations. *9th International Electric Drives Production Conference (EDPC)*, Esslingen, Germany, 2019. Pp. 1–5.